



## ATLAS CONF Note

ATLAS-CONF-2017-38

22nd May 2017



# Search for supersymmetry in events with $b$ -tagged jets and missing transverse momentum in $pp$ collisions at $\sqrt{s} = 13$ TeV with the ATLAS detector

The ATLAS Collaboration

A search for the supersymmetric partner of the Standard Model bottom and top quarks is presented. The search uses  $36.1 \text{ fb}^{-1}$  of  $pp$  collision data at  $\sqrt{s} = 13$  TeV collected by the ATLAS experiment at the Large Hadron Collider. Direct production of pairs of bottom and top squarks ( $\tilde{b}_1$  and  $\tilde{t}_1$ ) is searched for in final states with  $b$ -tagged jets and missing transverse momentum. Distinctive selections are defined with either no charged leptons (electrons and muons) in the final state, or one charged lepton. The zero-lepton selection targets models in which the  $\tilde{b}_1$  is the lightest squark and decays via  $\tilde{b}_1 \rightarrow b\tilde{\chi}_1^0$ , where  $\tilde{\chi}_1^0$  is the lightest neutralino. The one-lepton final state targets models where bottom or top squarks are produced and can decay into multiple channels,  $\tilde{b}_1 \rightarrow b\tilde{\chi}_1^0$  and  $\tilde{b}_1 \rightarrow t\tilde{\chi}_1^\pm$ , or  $\tilde{t}_1 \rightarrow t\tilde{\chi}_1^0$  and  $\tilde{t}_1 \rightarrow b\tilde{\chi}_1^\pm$ , where  $\tilde{\chi}_1^\pm$  is the lightest chargino and the mass difference  $m_{\tilde{\chi}_1^\pm} - m_{\tilde{\chi}_1^0}$  is set to 1 GeV. No excess above the expected Standard Model background yields is observed. Exclusion limits at 95% confidence level on the mass of the bottom squark are derived in various supersymmetry-inspired simplified models.

## Contents

<b>1</b>	<b>Introduction</b>	<b>2</b>
<b>2</b>	<b>ATLAS detector</b>	<b>4</b>
<b>3</b>	<b>Data and simulated event samples</b>	<b>4</b>
<b>4</b>	<b>Event reconstruction</b>	<b>6</b>
<b>5</b>	<b>Event selection</b>	<b>8</b>
5.1	Discriminating variables	8
5.2	Zero-lepton channel selections	10
5.3	One-lepton channel selections	11
<b>6</b>	<b>Background estimation</b>	<b>12</b>
6.1	Background estimation in the zero-lepton signal regions	13
6.2	Background estimation in the one-lepton signal regions	15
6.3	Validation regions	16
<b>7</b>	<b>Systematic uncertainties</b>	<b>18</b>
<b>8</b>	<b>Results and interpretation</b>	<b>21</b>
<b>9</b>	<b>Conclusion</b>	<b>26</b>

## 1 Introduction

Supersymmetry (SUSY) [1–6] provides an extension of the Standard Model (SM) that solves the hierarchy problem [7–10] by introducing partners of the known bosons and fermions. In the framework of the  $R$ -parity-conserving models, SUSY particles are produced in pairs and the lightest supersymmetric particle (LSP) is stable, providing a possible candidate for dark matter [11, 12]. In a large variety of models the LSP is the lightest neutralino ( $\tilde{\chi}_1^0$ ). Naturalness considerations [13, 14] suggest that the supersymmetric partners of the third-generation SM quarks are the lightest coloured supersymmetric particles. This may lead to the lightest bottom squark ( $\tilde{b}_1$ ) and top squark ( $\tilde{t}_1$ ) mass eigenstates<sup>1</sup> being significantly lighter than the other squarks and the gluinos. As a consequence,  $\tilde{b}_1$  and  $\tilde{t}_1$  could be pair-produced with relatively large cross-sections at the Large Hadron Collider (LHC).

This paper presents a search for the direct pair production of bottom and top squarks decaying into final states with jets, two of them originating from the fragmentation of  $b$ -quarks ( $b$ -jets), and missing transverse momentum ( $\mathbf{p}_T^{\text{miss}}$ , whose magnitude is referred to as  $E_T^{\text{miss}}$ ). The dataset analysed corresponds to  $36.1 \text{ fb}^{-1}$  of proton–proton ( $pp$ ) collisions at  $\sqrt{s} = 13 \text{ TeV}$  collected by the ATLAS experiment during Run-2 of the LHC in 2015 and 2016. The third generation squarks are assumed to decay to the lightest neutralino (LSP) directly or through one intermediate stage. The search targets models inspired by the minimal supersymmetric extension of the SM (MSSM) [15–17], where the  $\tilde{b}_1$  exclusively decays as

---

<sup>1</sup> Scalar partners of the left-handed and right-handed chiral components of the bottom quark ( $\tilde{b}_{\text{L,R}}$ ) or top quark ( $\tilde{t}_{\text{L,R}}$ ) mix to form mass eigenstates for which  $\tilde{b}_1$  and  $\tilde{t}_1$  are defined as the lighter of the two.

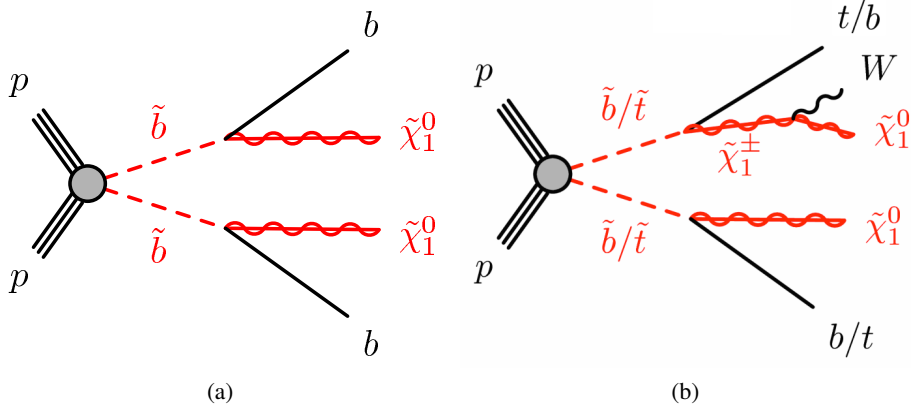


Figure 1: Diagrams illustrating the signal scenarios considered for the pair production of bottom and top squarks targeted by the (a) zero-lepton and (b) one-lepton channel selections. In (a) bottom squarks decay to a bottom-quark and the lightest neutralino. In (b), decays via intermediate charginos compete. If the mass difference  $\Delta m(\tilde{\chi}_1^\pm, \tilde{\chi}_1^0)$  is small,  $W$  from chargino decays are off-shell.

$\tilde{b}_1 \rightarrow b\tilde{\chi}_1^0$  or where two decay modes for the bottom (top) squark are allowed and direct decays to the LSP compete with decays via an intermediate chargino ( $\tilde{\chi}_1^\pm$ ) state,  $\tilde{b}_1 \rightarrow b\tilde{\chi}_1^0$  and  $\tilde{b}_1 \rightarrow t\tilde{\chi}_1^\pm$  ( $\tilde{t}_1 \rightarrow t\tilde{\chi}_1^0$  and  $\tilde{t}_1 \rightarrow b\tilde{\chi}_1^\pm$ ). In this case it is assumed that the  $\tilde{\chi}_1^\pm$  is the next-to-lightest supersymmetric particle (NLSP) and is almost degenerate with  $\tilde{\chi}_1^0$ , such that other decay products have too low momenta to be efficiently reconstructed. The first set of models lead to final state events for bottom-squark pair production characterized by the presence of two  $b$ -jets,  $E_T^{\text{miss}}$  and no charged leptons ( $\ell = e, \mu$ ), referred to as zero-lepton channel (Figure 1(a)). For mixed decays (direct or through an intermediate stage), the final state of bottom- and top-squark pair production depends on the branching ratio of the competing decay modes. If they are equally probable, a large fraction of signal events is characterised by the presence of a top quark, a bottom quark, and neutralinos. Hadronic decays of the top-quark are targeted by the zero-lepton channel, whilst a dedicated selection requiring one charged lepton, two  $b$ -jets and  $E_T^{\text{miss}}$  is developed for leptonic decays of the top-quark, referred to as one-lepton channel (Figure 1(b)). A statistical combination of the two channels is performed when interpreting the results in terms of exclusion limits on the third generation squark masses.

Previous searches for  $\tilde{b}_1 \rightarrow b\tilde{\chi}_1^0$  with the  $\sqrt{s} = 13$  TeV LHC Run-2 dataset at ATLAS and CMS have set exclusion limits at 95% confidence level (CL) on  $\tilde{b}_1$  masses in such scenarios. For  $\tilde{\chi}_1^0$  masses around 100 GeV, limits at 95% to 840 GeV and 960 GeV have been reported by the ATLAS [18] and CMS [19] collaborations, respectively, using  $3.2 \text{ fb}^{-1}$ (ATLAS) and  $35.9 \text{ fb}^{-1}$ (CMS) of data. Searches for the mixed decay models were performed by ATLAS using the Run-1  $\sqrt{s} = 8$  TeV dataset and resulted in exclusion limits on the third generation squark mass of up to 550 GeV depending on the branching ratio of the competing decay modes [20].

## 2 ATLAS detector

The ATLAS detector [21] is a multi-purpose particle physics detector with a forward-backward symmetric cylindrical geometry and nearly  $4\pi$  coverage in solid angle.<sup>2</sup> The inner tracking detector consists of pixel and silicon microstrip detectors covering the pseudorapidity region  $|\eta| < 2.5$ , surrounded by a transition radiation tracker which enhances electron identification in the region  $|\eta| < 2.0$ . Between Run-1 and Run-2, a new inner pixel layer, the Insertable B-Layer (IBL) [22], was inserted at a mean sensor radius of 3.3 cm. The inner detector is surrounded by a thin superconducting solenoid providing an axial 2 T magnetic field and by a fine-granularity lead/liquid-argon (LAr) electromagnetic calorimeter covering  $|\eta| < 3.2$ . A steel/scintillator-tile calorimeter provides hadronic coverage in the central pseudorapidity range ( $|\eta| < 1.7$ ). The endcap and forward regions ( $1.5 < |\eta| < 4.9$ ) of the hadronic calorimeter are made of LAr active layers with either copper or tungsten as the absorber material. An extensive muon spectrometer with an air-core toroid magnet system surrounds the calorimeters. Three layers of high-precision tracking chambers provide coverage in the range  $|\eta| < 2.7$ , while dedicated fast chambers allow triggering in the region  $|\eta| < 2.4$ . The ATLAS trigger system consists of a hardware-based level-1 trigger followed by a software-based high-level trigger (HLT) [23].

## 3 Data and simulated event samples

The data used in this analysis were collected by the ATLAS detector in  $pp$  collisions at the LHC with a centre-of-mass energy of 13 TeV and a 25 ns proton bunch crossing interval during 2015 and 2016. The full dataset corresponds to an integrated luminosity of  $36.1 \text{ fb}^{-1}$  after requiring that all detector subsystems were operational during data recording. The uncertainty in the combined 2015+2016 integrated luminosity is 3.2%. It is derived following a methodology similar to that detailed in Ref. [24] from a preliminary calibration of the luminosity scale using  $x - y$  beam-separation scans performed in August 2015 and May 2016. Each event includes on average 13.7 and 24.9 inelastic  $pp$  collisions (“pileup”) in the same bunch crossing in the 2015 and 2016 dataset, respectively. In the zero-lepton channel events are required to pass an  $E_T^{\text{miss}}$  trigger [25]. These triggers are fully efficient for events passing the preselection defined in Section 5, which requires the offline reconstructed  $E_T^{\text{miss}}$  to exceed 200 GeV. Events in the one-lepton channel, as well as events used for control regions, are selected online by a trigger requiring the presence of one electron or muon. The online selection thresholds are such that a plateau of the efficiency is reached for charged lepton transverse momenta of 27 GeV.

Monte Carlo (MC) samples of simulated events are used to model the signal and to aid in the estimation of SM background processes, except multijet processes which are estimated from data only. All simulated events are passed through the full detector simulation using GEANT4 [26], or through a faster simulation based on a parameterization [27] for the calorimeter response and GEANT4 for the other detector systems. The simulated events are reconstructed with the same algorithm as that used for data.

---

<sup>2</sup> ATLAS uses a right-handed coordinate system with its origin at the nominal interaction point in the centre of the detector. The positive  $x$ -axis is defined by the direction from the interaction point to the centre of the LHC ring, with the positive  $y$ -axis pointing upwards, while the beam direction defines the  $z$ -axis. Cylindrical coordinates  $(r, \phi)$  are used in the transverse plane,  $\phi$  being the azimuthal angle around the  $z$ -axis. The pseudorapidity  $\eta$  is defined in terms of the polar angle  $\theta$  by  $\eta = -\ln(\tan(\theta/2))$ . Rapidity is defined as  $y = 0.5 \ln[(E + p_z)/(E - p_z)]$  where  $E$  denotes the energy and  $p_z$  is the component of the momentum along the beam direction.

SUSY signal samples are generated with `MADGRAPH5_aMC@NLO` [28] v2.2.3 at leading-order (LO) and interfaced to `PYTHIA` 8.186 [29] with the A14 [30] set of parameters (tune) for the modelling of the parton showering (PS), hadronization and underlying event. The matrix element (ME) calculation is performed at tree level and includes the emission of up to two additional partons. The ME-PS matching is done using the CKKW-L [31] prescription, with a matching scale set to one quarter of the third generation squark mass. The NNPDF23LO [32] parton density function (PDF) set is used. The cross-sections used to evaluate the signal yields are calculated to next-to-leading-order (NLO) accuracy in the strong coupling constant, adding the resummation of soft gluon emission at next-to-leading-logarithmic accuracy (NLO+NLL) [33–35]. The nominal cross-section and uncertainty are taken as the midpoint and half-width of an envelope of cross-section predictions using different PDF sets and factorisation and renormalisation scales, as described in Ref. [36].

SM background samples are simulated using different MC generator programs depending on the process. The generation of  $t\bar{t}$  pairs and single top-quarks in the  $Wt$  and  $s$ -channels is made using the PowHEG-Box [37] v2 generator with the CT10 [38] PDF set for the matrix element calculations. Electroweak  $t$ -channel single top-quark events are generated using the PowHEG-Box v1 generator. For all processes involving top quarks, top-quark spin correlations are preserved. The parton shower, fragmentation, and the underlying event are simulated using `PYTHIA` 6.428 [39] with the CTEQ6L1 PDF set. The  $h_{damp}$  parameter in PowHEG, which controls the  $p_T$  of the first additional emission beyond the Born level and thus regulates the  $p_T$  of the recoil emission against the  $t\bar{t}$  system, is set to the mass of the top quark ( $m_{top} = 172.5$  GeV). All events with at least one leptonically decaying  $W$  boson are included. Fully hadronic  $t\bar{t}$  and single top events do not contain sufficient  $E_T^{\text{miss}}$  to contribute significantly to the background. The  $t\bar{t}$  samples are normalized to their next-to-NLO (NNLO) cross-section including the resummation of soft gluon emission at next-to-NLL accuracy using `Top++2.0` [40]. Samples of single-top-quark production are normalized to the NLO cross-sections reported in Refs. [41–43] for the  $s$ -,  $t$ - and  $Wt$ -channels, respectively.

Events containing  $W$  or  $Z$  bosons with associated jets, including jets from the fragmentation of  $b$ - and  $c$ -quarks, are simulated using the `SHERPA` v2.2.1 [44] generator. Matrix elements are calculated for up to two additional partons at NLO and four partons at LO using the `COMIX` [45] and `OPENLOOPS` [46] matrix element generators and merged with the `SHERPA` PS [47] using the ME+PS@NLO prescription [48]. The NNPDF30NNLO [32] PDF set is used in conjunction with a dedicated PS tune developed by the `SHERPA` authors. Additional `SHERPA`  $Z$ +jets samples were produced with similar settings but with up to four partons LO, for the  $\gamma$ +jets studies detailed in Section 6. The  $W/Z$ +jets events are normalized to their NNLO QCD theoretical cross-sections [49].

Diboson processes are also simulated using the `SHERPA` generator using the NNPDF30NNLO PDF set in conjunction with a dedicated PS tune developed by the `SHERPA` authors. They are calculated for up to one ( $ZZ$ ) or zero ( $WW, WZ$ ) additional partons at NLO and up to three additional partons at LO. Additional contributions to the SM backgrounds in the signal regions arise from the production of  $t\bar{t}$  pairs in association with  $W/Z/h$  bosons and possibly additional jets. The production of  $t\bar{t}$  pairs in association with electroweak vector bosons  $W$  and  $Z$  and Higgs boson is modeled by samples generated at NLO using `MADGRAPH5_aMC@NLO` v2.2.3 and showered with `PYTHIA` v8.212. Other potential sources of backgrounds, such as the production of three or four top quarks or three gauge bosons, are found to be negligible.

For all samples, except the ones generated using `SHERPA`, the `EvtGEN` v1.2.0 program [50] is used to simulate the properties of the bottom and charm-hadron decays. All `PYTHIA` v6.428 samples use the `PERUGIA2012` [51] tune for the underlying event, while `PYTHIA` v8.186 and `HERWIG++` showering are run

with the A14 and UEEE5 [52] underlying-event tunes, respectively. In-time and out-of-time pileup interactions from the same or nearby bunch-crossings are simulated by overlaying additional  $pp$  collisions generated by PYTHIA v8.186, and the MSTW2008LO [53] parton distribution function set, superimposed onto the hard scattering events to reproduce the observed distribution of the average number of interactions per bunch crossing [54].

Several samples produced without detector simulation are employed to derive systematic uncertainties associated with the specific configuration of the MC generators used for the nominal SM background samples. They include variations of the renormalization and factorization scales, the CKKW-L matching scale, as well as different PDF sets and fragmentation/hadronization models. Details of the MC modelling uncertainties are discussed in Section 7.

## 4 Event reconstruction

The search for pair production of bottom and top squarks is based on two distinctive selections of events with  $b$ -jets and large missing transverse momentum, with either no charged leptons in the final state, or requiring exactly one electron or muon. For the zero-lepton channel selection, events containing charged leptons are explicitly vetoed in the signal and validation regions. Events characterized by the presence of exactly one electron or muon with transverse momentum above 27 GeV are retained in the one-lepton selection and are also used to define control regions for the zero-lepton channel. Finally, same-flavour opposite-sign (SFOS) two-lepton (electron or muon) events with dilepton invariant mass near the  $Z$  boson mass are used for control regions employed to aid in the estimate of the  $Z$ +jets background. The details of the selections and the reconstructed objects as well as the overlap removal procedure applied to prevent their double-counting are given below.

Selected events are required to have a reconstructed primary vertex consistent with the beamspot envelope and to consist of at least two tracks in the inner detector with  $p_T > 0.4$  GeV. When more than one such vertex is found the one with the largest sum of the squares of transverse momenta of associated tracks [55] is chosen.

Jet candidates are reconstructed from three-dimensional energy clusters [56] in the calorimeter using the anti- $k_t$  jet algorithm [57] with a distance parameter of 0.4. Each topological cluster’s energy is calibrated to the electromagnetic scale prior to jet reconstruction. The reconstructed jets are then calibrated to the particle level by the application of a jet energy scale (JES) derived from  $\sqrt{s} = 13$  TeV data and simulations [58]. Quality criteria are imposed to identify jets arising from non-collision sources or detector noise and any event containing such a jet is removed [59]. Further track-based selections are applied to reject jets with  $p_T < 60$  GeV and  $|\eta| < 2.4$  that originate from pile-up interactions [60] and the expected event average energy contribution from pile-up clusters is subtracted using the jet area method [61]. Jets are classified as “baseline” and “signal”. Baseline jets are required to have  $p_T > 20$  GeV and  $|\eta| < 4.8$ . Signal jets, selected after resolving overlaps with electrons and muons, are required to pass the stricter requirement of  $p_T > 35$  GeV and  $|\eta| < 2.8$ .

Jets are identified as  $b$ -jets if tagged by a multivariate algorithm which uses information about the impact parameters of inner detector tracks matched to the jet, the presence of displaced secondary vertices, and the reconstructed flight paths of  $b$ - and  $c$ -hadrons inside the jet [62]. The  $b$ -tagging working point with a 77% efficiency, as determined in a sample of simulated  $t\bar{t}$  events, was chosen as part of the optimization procedure. The corresponding rejection factors against jets originating from  $c$ -quarks and from light

quarks and gluons at this working point are 6.2 and 134, respectively [63]. To compensate for differences between data and MC simulation in the  $b$ -tagging efficiencies and mis-tag rates, correction factors derived from data and are applied to the samples of simulated events [62]. Candidate  $b$ -jets are required to have  $p_T > 50$  GeV and  $|\eta| < 2.5$ .

Electron candidates are reconstructed from energy clusters in the electromagnetic calorimeter matched to a track in the inner detector and are required to satisfy a set of “loose” quality criteria [64–66]. They are also required to lie within the fiducial volume  $|\eta| < 2.47$ . Muon candidates are reconstructed from matching tracks in the inner detector with tracks in the muon spectrometer. Events containing one or more muon candidates that have a transverse (longitudinal) impact parameter with respect to the primary vertex larger than 0.2 mm (1 mm) are rejected to suppress muons from cosmic rays. Muon candidates are also required to satisfy “medium” quality criteria [67] and have  $|\eta| < 2.5$ . All electron and muon candidates must have  $p_T > 10$  GeV. Lepton candidates remaining after resolving the overlap with baseline jets (see next paragraph) are called “baseline” leptons. In the control and signal regions where lepton identification is required, “signal” leptons are chosen from the baseline set with  $p_T > 27$  GeV to ensure full efficiency of the trigger and are required to be isolated from other objects using a criterion designed to accept at least 95% of leptons from  $Z$  boson decays as detailed in Ref. [68]. The angular separation between the lepton and the  $b$ -jet arising from a leptonically decaying top quark will narrow as the top  $p_T$  increases. This increased collimation is accounted for by varying the radius of the isolation cone as  $\text{max}(0.2, 10 \text{ GeV}/p_T^{\text{lep}})$ , where  $p_T^{\text{lep}}$  is the lepton  $p_T$ . Signal electrons are further required to satisfy “tight” quality criteria. Electrons (muons) are matched to the primary vertex by requiring the transverse impact parameter ( $d_0$ ) to satisfy  $|d_0/\sigma(d_0)| < 5$  (3), and the longitudinal impact parameter ( $z_0$ ) to satisfy  $|z_0 \sin \theta| < 0.5$  mm for both the electrons and muons. The MC events are corrected to account for differences in the lepton trigger, reconstruction and identification efficiencies between data and MC simulation.

The sequence to resolve overlapping objects begins by removing electron candidates sharing an inner detector track with a muon candidate. Next, jet candidates within  $\Delta R = \sqrt{(\Delta y)^2 + (\Delta \phi)^2} = 0.2$  of an electron candidate are discarded, unless the jet is  $b$ -tagged, in which case the electron is discarded since it is likely to originate from a semileptonic  $b$ -hadron decay. Finally, electrons are discarded if they lie within  $\Delta R = 0.4$  of a jet, whilst muons with  $p_T$  below (above) 50 GeV are discarded if they lie within  $\Delta R = 0.4$  ( $\Delta R = \text{min}(0.4, 0.04 + 10 \text{ GeV}/p_T)$ ) of any remaining jet, except for the case where the number of tracks associated with the jet is less than three.

The missing transverse momentum is defined as the negative vector sum of the  $p_T$  of all selected and calibrated physics objects in the event, with an extra term added to account for soft energy in the event which is not associated with any of the selected objects. This soft term is calculated from inner detector tracks with  $p_T$  above 0.4 GeV matched to the primary vertex to make it more robust against pile-up contamination [69, 70].

Reconstructed photons are not used in the main signal event selections but are selected in the regions employed in one of the alternative methods used to check the  $Z$ +jets background, as explained in Section 6. Photon candidates are required to have  $p_T > 10$  GeV and  $|\eta| < 2.37$ , whilst being outside the transition region  $1.37 < |\eta| < 1.52$ , to satisfy the tight photon shower shape and electron rejection criteria [71]. The photons used in this analysis are further required to have  $p_T > 130$  GeV and to be isolated.

## 5 Event selection

Two sets of signal regions (SRs) are defined and optimised to target different third generation squark decay modes and mass hierarchies of the particles involved. The zero-lepton channel SRs (b0L) are set to maximize the efficiency to retain bottom-squark pair production events where  $\tilde{b}_1 \rightarrow b\tilde{\chi}_1^0$ . The one-lepton channel selections (b1L) target SUSY models where bottom squarks decay with significant branching ratio as  $\tilde{b}_1 \rightarrow t\tilde{\chi}_1^\pm$  and the lightest chargino is almost degenerate with the lightest neutralino. Under these assumptions, the final decay products of the off-shell  $W$  boson from  $\tilde{\chi}_1^\pm \rightarrow \tilde{\chi}_1^0 W^*$  are too soft to be detected. If the branching ratio of the two competing decay modes ( $b\tilde{\chi}_1^0, t\tilde{\chi}_1^\pm$ ) is around 50%, the final state of the largest fraction of signal events is characterised by the presence of a top quark, a bottom quark, and neutralinos escaping the detector. Similarly,  $\tilde{t}_1$  pair production can lead to an equivalent final state if  $\tilde{t}_1 \rightarrow t\tilde{\chi}_1^0$  and  $\tilde{t}_1 \rightarrow b\tilde{\chi}_1^\pm$  decay modes compete.

### 5.1 Discriminating variables

Several kinematic variables and angular correlations, built from the physics objects defined in the previous section, are employed to discriminate SUSY from SM background events and are reported below. In the following signal jets are used and are ordered according to decreasing  $p_T$ .

- $\min[\Delta\phi(\text{jet}_{1-4}, E_T^{\text{miss}})]$ ,  $\min[\Delta\phi(\text{jet}_{1-2}, E_T^{\text{miss}})]$ : These variables are the minimum  $\Delta\phi$  between any of the leading jets and the missing transverse momentum vector. The background from multijet processes is characterised by small values of this variable. Depending on the signal regions, four or two jets are used.
- $H_T$  : This is defined as the scalar sum of the  $p_T$  of all jets in the event

$$H_T = \sum_i (p_T^{\text{jet}})_i,$$

where the number of jets involved depends on the signal region. In addition, the modified form of  $H_T$ , referred to as the  $H_{T4}$  variable, is used to reject events with extra-jet activity in signal regions targeting models characterized by small mass splitting between the bottom squark and the neutralino. In  $H_{T4}$  the sum starts on the fourth jet (if any).

- $m_{\text{eff}}$  : This is defined as the scalar sum of the  $p_T$  of the leading four jets and the  $E_T^{\text{miss}}$ , i.e.:

$$m_{\text{eff}} = \sum_{i \leq 4} (p_T^{\text{jet}})_i + E_T^{\text{miss}}.$$

The  $m_{\text{eff}}$  observable is correlated with the mass of the pair-produced SUSY particles and is employed as discriminating variable in some of the zero-lepton and one-lepton channels selections, as well as in the computation of other complex observables.

- $E_T^{\text{miss}}/m_{\text{eff}}$ ,  $E_T^{\text{miss}}/\sqrt{H_T}$  : The first ratio is the fraction of the  $E_T^{\text{miss}}$  over the  $m_{\text{eff}}$ , while the second emulates the global  $E_T^{\text{miss}}$  significance, given that the  $E_T^{\text{miss}}$  resolution scales approximately with the square root of the total hadronic energy in the event. Events with low  $E_T^{\text{miss}}$  significance are rejected as it is most probable that  $E_T^{\text{miss}}$  arises from jets mis-measurements, caused by instrumental and resolution effects.

- $m_{jj}$  : This is a selection on the invariant mass of the leading two jets. In events where at least one of the leading jets is  $b$ -tagged, this variable aids in reducing the contamination from  $t\bar{t}$  events. It is referred to as  $m_{bb}$  for events with two  $b$ -tagged jets.
- $m_T$ : The event transverse mass  $m_T$  is defined as  $m_T = \sqrt{2p_T^{\text{lep}}E_T^{\text{miss}} - 2\mathbf{p}_T^{\text{lep}} \cdot \mathbf{p}_T^{\text{miss}}}$  and is used in one-lepton control and signal regions to reduce  $W+\text{jets}$  and  $t\bar{t}$  background events.
- $m_{b\ell}^{\min}$  : The minimum invariant mass of the lepton and one of the two  $b$ -jets is defined as:

$$m_{b\ell}^{\min} = \min_{i=1,2} (m_{\ell b_i}).$$

This variable is bound from above to  $\sqrt{m_t^2 - m_W^2}$  for  $t\bar{t}$  production, and it is used to distinguish  $t\bar{t}$  contributions from single-top-quark production events from the  $Wt$  channel in the one-lepton control regions.

- Contratransverse mass ( $m_{\text{CT}}$ ) [72]: This is the main discriminating variable in most of the zero-lepton channel signal regions [73]. It is used to measure the masses of pair-produced semi-invisibly decaying heavy particles. For two identical decays of heavy particles (e.g. the bottom squarks for exclusive decays as  $\tilde{b}_1 \rightarrow b\tilde{\chi}_1^0$ ) into two visible particles  $v_1$  and  $v_2$  (the  $b$ -quarks), and two invisible particles  $X_1$  and  $X_2$  (the  $\tilde{\chi}_1^0$  for the signal),  $m_{\text{CT}}$  is defined as

$$m_{\text{CT}}^2(v_1, v_2) = [E_T(v_1) + E_T(v_2)]^2 - [\mathbf{p}_T(v_1) - \mathbf{p}_T(v_2)]^2,$$

with  $E_T = \sqrt{p_T^2 + m^2}$ , and it has a kinematical endpoint at  $m_{\text{CT}}^{\max} = \frac{m_i^2 - m_X^2}{m_i}$  where  $i$  is the initially pair produced particle. This variable is extremely effective in suppressing the top-quark pair production background ( $i = t, X = W$ ), for which the endpoint is at 135 GeV.

- $\min[m_T(\text{jet}_{1-4}, E_T^{\text{miss}})]$  : It is the minimum transverse mass of the leading four jets and the  $E_T^{\text{miss}}$  in the event. For signal scenarios with low values of  $m_{\text{CT}}^{\max}$ , this kinematic variable is an alternative discriminating variable to reduce the  $t\bar{t}$  background.
- $am_{\text{T2}}$ : The asymmetric transverse mass [74, 75] is a kinematic variable which can be used to separate processes in which two decays giving missing transverse momentum occur and it is the main discriminant observable in the one-lepton channel signal regions. The  $am_{\text{T2}}$  definition is based on the transverse mass ( $m_{\text{T2}}$ ) [76]:

$$m_{\text{T2}}^2(\chi) = \min_{\mathbf{q}_T^{(1)} + \mathbf{q}_T^{(2)} = \mathbf{p}_T^{\text{miss}}} \left[ \max \left\{ m_T^2(\mathbf{p}_T(v_1), \mathbf{q}_T^{(1)}; \chi), m_T^2(\mathbf{p}_T(v_2), \mathbf{q}_T^{(2)}; \chi) \right\} \right],$$

where  $\mathbf{p}_T(v_i)$  are reconstructed transverse momenta vectors and  $\mathbf{q}_T^{(i)}$  represent the missing transverse momenta from the two decays, with a total missing transverse momentum,  $\mathbf{p}_T^{\text{miss}}$ ;  $\chi$  is a free parameter representing the unknown mass of the invisible particles – here assumed to be zero. The  $a$  in  $am_{\text{T2}}$  indicates that the two visible decay legs are asymmetric, i.e. not composed of the same particles.

In the case of events with one lepton (electron or muon) and two  $b$ -jets, the  $m_{\text{T2}}$  is calculated for different values of  $\mathbf{p}_T(v_1)$  and  $\mathbf{p}_T(v_2)$ , by grouping the lepton and the two  $b$ -jets into two visible objects  $v_1$  and  $v_2$ . The lepton needs to be paired with one of the two  $b$ -jets and the choice is driven by the value of  $m_{bl}$  (n) - the invariant mass of the  $n^{\text{th}}$   $b$ -tagged jet and the lepton. If the two particles are correctly coupled, this value has an upper bound given by the top quark mass. The value of  $am_{\text{T2}}$  is thus computed accordingly:

- If  $m_{bl}$  (1) and  $m_{bl}$  (2) are both  $> 170$  GeV, none of the two couplings is compatible with the  $b$ -jet and the lepton originating from a top decay, therefore the event is rejected as all control, validation and signal regions contain a cut on the minimum value of  $m_{bl}$  to be  $< 170$  GeV.
- If  $m_{bl}$  (1) is  $< 170$  GeV and  $m_{bl}$  (2) is  $> 170$  GeV,  $am_{T2}$  is calculated with  $v_1 = b_1 + l$  and  $v_2 = b_2$ . This is done because only the first pairing is compatible with a top quark decay.
- Similarly, if  $m_{bl}$  (1) is  $> 170$  GeV and  $m_{bl}$  (2) is  $< 170$  GeV,  $am_{T2}$  is calculated with  $v_1 = b_1$  and  $v_2 = b_2 + l$ .
- If  $m_{bl}$  (1) and  $m_{bl}$  (2) are both  $< 170$  GeV,  $am_{T2}$  is calculated in both configurations and its value is taken to be the minimum of the two. This must be done since according to the  $m_{bl}$  check both pairings would be acceptable.

- $\mathcal{A}$  : This is the  $p_T$  asymmetry of the leading two jets and is defined as:

$$\mathcal{A} = \frac{p_T(j_1) - p_T(j_2)}{p_T(j_1) + p_T(j_2)}.$$

The  $\mathcal{A}$  variable is employed in scenarios where the mass splitting between the bottom squark and the neutralino is small ( $< 20$  GeV) and the selection exploits the presence of a high momentum jet from initial state radiation.

## 5.2 Zero-lepton channel selections

The selection criteria for the zero-lepton channel SRs are summarized in Table 1 and have the main requirement of no baseline leptons with  $p_T > 10$  GeV. To exploit the kinematic properties over the large range of  $\tilde{b}_1$  and  $\tilde{\chi}_1^0$  masses explored, three sets of SRs have been defined.

The b0L-SRA regions are optimized to be sensitive to models with large mass splitting between the  $\tilde{b}_1$  and the  $\tilde{\chi}_1^0$ ,  $\Delta m(\tilde{b}_1, \tilde{\chi}_1^0) > 250$  GeV. Incremental thresholds are applied on the main discriminating variable,  $m_{CT}$ , resulting in three overlapping regions ( $m_{CT} > 350, 450$  and  $550$  GeV). Only events with  $E_T^{\text{miss}} > 250$  GeV are retained to ensure full efficiency of the trigger and comply with the expected signal topology. Two high  $p_T$   $b$ -tagged jets are required whilst contamination from backgrounds with high jet multiplicity, particularly  $t\bar{t}$  production, is suppressed by vetoing events with a fourth jet with  $p_T > 50$  GeV. To discriminate against multijet background, events where  $E_T^{\text{miss}}$  is aligned with a jet in the transverse plane are rejected by requiring  $\Delta\phi_{\text{min}}^j > 0.4$ , and  $E_T^{\text{miss}}/m_{\text{eff}} > 0.25$ . A selection on the invariant mass of the two  $b$ -jets ( $m_{bb} > 200$  GeV) is applied to further enhance the signal yield over the SM background contributions.

The b0L-SRB region targets intermediate mass splitting between  $\tilde{b}_1$  and  $\tilde{\chi}_1^0$ ,  $50 < \Delta m(\tilde{b}_1, \tilde{\chi}_1^0) < 250$  GeV. In these scenarios, the selections based on the  $m_{CT}$  and  $m_{bb}$  variables are no longer effective and the variable  $\min[m_T(\text{jet}_{1-4}, E_T^{\text{miss}})]$  is employed to reduce SM background contributions from  $t\bar{t}$  production, with events selected if  $\min[m_T(\text{jet}_{1-4}, E_T^{\text{miss}})] > 250$  GeV. Up to four jets with  $p_T > 35$  GeV are allowed, to reduce additional hadronic activity in the selected events. As opposed to the b0L-SRA criteria, no veto of the fourth jet  $p_T$  is applied. A series of selections on the azimuthal angle between the two  $b$ -tagged jets and the  $E_T^{\text{miss}}$  are implemented ( $|\Delta\phi(b_1, E_T^{\text{miss}})| < 2.0$  and  $|\Delta\phi(b_2, E_T^{\text{miss}})| < 2.5$ ) to reduce  $Z+jets$  background events.

Finally, the b0L-SRC region targets events where a bottom squark pair is produced in association with a jet from initial-state radiation (ISR). This selection provides sensitivity to models with a small mass difference between the  $\tilde{b}_1$  and the  $\tilde{\chi}_1^0$ ,  $\Delta m(\tilde{b}_1, \tilde{\chi}_1^0) < 50$  GeV, such that a boosted bottom squark pair would satisfy the trigger requirements. To suppress efficiently  $t\bar{t}$  and  $W$ +jets backgrounds, events are selected with one high  $p_T$  non- $b$ -tagged jet and  $E_T^{\text{miss}} > 500$  GeV such that  $\Delta\phi(j_1, E_T^{\text{miss}}) > 2.5$ . Stringent requirements on the minimum azimuthal distance between the jets and  $E_T^{\text{miss}}$  are found to be not suited for these scenarios where  $b$ -jets have softer momenta and are possibly aligned to  $E_T^{\text{miss}}$ . A large asymmetry  $\mathcal{A}$  is required to reduce multijet background while loosening the selection on the minimum azimuthal distance between the jets and  $E_T^{\text{miss}}$  to  $\min[\Delta\phi(\text{jet}_{1-2}, E_T^{\text{miss}})] > 0.2$ , while the  $p_T$  threshold on signal jets is relaxed to 20 GeV.

Table 1: Summary of the event selection in each signal region for the zero-lepton channel. The term lepton is used in the table to refer to baseline electrons and muons. Jets ( $j_1, j_2, j_3, j_4$  and  $j_5$ ) are labelled with an index corresponding to their decreasing order in  $p_T$ .

	b0L-SRAx	b0L-SRB	b0L-SRC
Lepton veto		No $e/\mu$ with $p_T > 10$ GeV after overlap removal	
$N_{\text{jets}}(p_T > 35 \text{ GeV})$	2-4	2-4	-
$N_{\text{jets}}(p_T > 20 \text{ GeV})$	-	-	2-5
$p_T(j_1) [\text{GeV}]$	$> 130$	$> 50$	$> 500$
$p_T(j_2) [\text{GeV}]$	$> 50$	$> 50$	$> 20$
$p_T(j_4) [\text{GeV}]$	$< 50$	-	-
$H_{\text{T4}} [\text{GeV}]$	-	-	$< 70$
$b$ -jets	$j_1$ and $j_2$	any 2	$j_2$ and ( $j_3$ or $j_4$ or $j_5$ )
$E_T^{\text{miss}} [\text{GeV}]$	$> 250$	$> 250$	$> 500$
$E_T^{\text{miss}}/m_{\text{eff}}$	$> 0.25$	-	-
$\min[\Delta\phi(\text{jet}_{1-4}, E_T^{\text{miss}})]$	$> 0.4$	$> 0.4$	-
$\min[\Delta\phi(\text{jet}_{1-2}, E_T^{\text{miss}})]$	-	-	$> 0.2$
$\Delta\phi(b_1, E_T^{\text{miss}})$	-	$< 2.0$	-
$\Delta\phi(b_2, E_T^{\text{miss}})$	-	$< 2.5$	-
$\Delta\phi(j_1, E_T^{\text{miss}})$	-	-	$> 2.5$
$m_{bb} [\text{GeV}]$	$> 200$	-	$> 200$
$m_{\text{CT}} [\text{GeV}]$	$> 350, 450, 550$	-	-
$m_T^{\text{min}}(\text{jet}_{1-4}, E_T^{\text{miss}}) [\text{GeV}]$	-	$> 250$	-
$m_{\text{eff}} [\text{TeV}]$	-	-	$> 1.3$
$\mathcal{A}$	-	-	$> 0.8$

### 5.3 One-lepton channel selections

The selection criteria for the one-lepton channel SRs are summarized in Table 2. Events are required to have exactly one signal electron or muon and no additional baseline leptons, two  $b$ -tagged jets and a large  $E_T^{\text{miss}}$ . Similarly to the zero-lepton channel, three sets of SRs are defined to maximize the sensitivity depending on the mass hierarchy between  $\tilde{b}_1(\tilde{t}_1)$  and  $\tilde{\chi}_1^\pm \approx \tilde{\chi}_1^0$ .

The b1L-SRA regions are optimized for models with large  $\Delta m(\tilde{b}_1, \tilde{\chi}_1^0)$ : events are required to have large  $E_T^{\text{miss}}$  and  $E_T^{\text{miss}}/\sqrt{H_T}$ , two  $b$ -tagged jets and  $\min[\Delta\phi(\text{jet}_{1-4}, E_T^{\text{miss}})]$  above 0.4 to reduce multijet background contributions to negligible levels. Requirements on the  $m_T$  and  $am_{T2}$  variables to be above 140 GeV and 250 GeV, respectively, are set to reject  $W+\text{jets}$  and  $t\bar{t}$  events whilst the selection on the invariant mass of the two  $b$ -jets ( $m_{bb} > 200$  GeV) is applied to further enhance the signal yield over the SM background contributions. Two incremental thresholds are finally applied on  $m_{\text{eff}}$  (600 and 750 GeV) to define two overlapping signal regions.

The b1L-SRB region is designed to be sensitive to compressed mass spectra, hence low  $m_{bb}$  is expected, and the selections on the  $m_T$  and  $am_{T2}$  variables must be relaxed to avoid loss of signal events. The  $\min[m_T(\text{bjet}, E_T^{\text{miss}})]$  is employed to discriminate signal from  $t\bar{t}$  events, the dominant SM background contribution.

A third region, referred to as b1L-SRA300-2j, is defined as b1L-SRAs but requiring no-extra jets beside the two  $b$ -jets and no threshold on  $m_{\text{eff}}$ . Such selection also targets SUSY models characterized by compressed mass spectra. It is kinematically similar to the signal region in the Run1 analysis [20] with a veto requirement on the number of jets with  $p_T > 50$  GeV.

Table 2: Summary of the event selection in each signal region for the one-lepton channel. The term lepton is used in the table to refer to signal electrons and muons. Jets ( $j_1, j_2, j_3$  and  $j_4$ ) are labelled with an index corresponding to their decreasing order in  $p_T$ .

	b1L-SRAx	b1L-SRA300-2j	b1L-SRB
Number of leptons ( $e, \mu$ )	1	1	1
$N_{\text{jets}}(p_T > 35 \text{ GeV})$	$\geq 2$	$= 2$	$\geq 2$
$b$ -jets	any 2	$j_1$ and $j_2$	any 2
$E_T^{\text{miss}}$ [GeV]	$> 200$	$> 200$	$> 200$
$E_T^{\text{miss}}/\sqrt{H_T}$ [ (GeV $^{\frac{1}{2}}$ )]	$> 8$	$> 8$	$> 8$
$m_{b\ell}^{\text{min}}$ [GeV]	$< 170$	$< 170$	$< 170$
$\min[\Delta\phi(\text{jet}_{1-4}, E_T^{\text{miss}})]$	$> 0.4$	–	$> 0.4$
$\min[\Delta\phi(\text{jet}_{1-2}, E_T^{\text{miss}})]$	–	$> 0.4$	–
$am_{T2}$ [GeV]	$> 250$	$> 250$	$> 200$
$m_T$ [GeV]	$> 140$	$> 140$	$> 120$
$m_{bb}$ [GeV]	$> 200$	$> 200$	$< 200$
$m_{\text{eff}}$ [GeV]	$> 600, 750$	$> 300$	$> 300$
$m_T^{\text{min}}(\text{bjet}_{1-2}, E_T^{\text{miss}})$ [GeV]	–	–	$> 200$
$\Delta\phi(b_1, E_T^{\text{miss}})$	–	–	$> 2.0$

## 6 Background estimation

Monte Carlo simulation is used to estimate the background yield in the signal regions. The MC prediction for the major backgrounds is normalized to data in control regions (CR) constructed to enhance a particular background and to be kinematically similar but mutually exclusive to the signal regions. The control regions are defined by explicitly requiring the presence of one or two leptons (electrons or muons) in the final state together with further selection criteria similar to those of the corresponding signal region. To

ensure that the b0L and b1L analyses can be statistically combined, the CRs associated to b0L and b1L SRs are mutually exclusive, with the exception of the single-top CR, where the same CR is used for both channels.

The SM background expectations are determined separately for each SR with a profile likelihood fit [77], referred to as background-only fit. The fit uses as a constraint the observed event yield in a set of associated CRs to adjust the normalisation of the main backgrounds, assuming that no signal is present. The inputs to the fit for each SR include the number of events observed in its associated CR and the number of events predicted by simulation in each region for all background processes. The latter are described by Poisson statistics. The systematic uncertainties in the expected values are included in the fit as nuisance parameters. They are constrained by Gaussian distributions with widths corresponding to the sizes of the uncertainties and are treated as correlated, when appropriate, between the various regions. The product of the various probability density functions forms the likelihood, which the fit maximises by adjusting the background normalisation and the nuisance parameters. Finally, the reliability of the MC extrapolation of the SM background estimate outside of the control regions is evaluated in several validation regions (VRs).

## 6.1 Background estimation in the zero-lepton signal regions

The main SM background in the b0L signal regions is the production of  $Z$ +jets followed by invisible decays of the  $Z$ -boson. The production of top-quark pairs, single top-quark and  $W$ +jets are also important background with their relative contribution depending on the specific SR considered. Full details of the CR definitions are given in Tables 3 and 4.

Three same-flavour opposite-sign (SFOS) two-lepton (electron or muon) control regions with dilepton invariant mass near the  $Z$  boson mass ( $76 < m_{\ell\ell} < 106$  GeV) and two  $b$ -tagged jets provide data samples dominated by  $Z$  boson production. Signal leptons are considered, with the threshold of the second lepton  $p_T$  loosened to 20 GeV. For these control regions, labelled in the following as b0L-CRzA, b0L-CRzB and b0L-CRzC, the  $p_T$  of the leptons is added vectorially to the  $\mathbf{p}_T^{\text{miss}}$  to mimic the expected missing transverse momentum spectrum of  $Z \rightarrow \nu\bar{\nu}$  events, and is indicated in the following as  $E_T^{\text{miss,cor}}$  (lepton corrected). In addition, a selection is applied on the uncorrected  $E_T^{\text{miss}}$  of the event, in order to further enhance the  $Z$  boson contribution.

Events with one charged lepton in the final state are used to define control regions dominated by  $W$ +jets and top-quark production by requiring either one or two  $b$ -tagged jets, respectively. Selections on the variable  $m_T$  are used to ensure that the lepton originates from a  $W$  decay. For the CRs corresponding to b0L-SRA, the contribution from  $t\bar{t}$  and single top-quark production are separated by applying the selection  $m_{bb} < 200$  GeV and  $m_{bb} > 200$  GeV, respectively. To further enhance the single top-quark contribution a selection on the minimum invariant mass of the lepton and one of the  $b$ -jets,  $m_{b\ell}^{\text{min}} > 170$  GeV is applied. For the CRs corresponding to b0L-SRB, selections on the azimuthal angle between the  $b$ -jets and the  $E_T^{\text{miss}}$  are applied to enhance the  $t\bar{t}$  and  $W$ +jets contributions, while the single top-quark background is estimated from MC. Finally for the CRs corresponding to the b0L-SRC, control regions are defined with one or two  $b$ -jets to enhance the  $t\bar{t}$  and  $W$ +jets contributions respectively, while single top-quark production is estimated using the MC normalization.

The contributions from diboson, multijet and rare backgrounds are minor and they are collectively called “Others” in the following. The dibosons and rare backgrounds are estimated from MC simulation for both the signal and the control regions and included in the fit procedure, and are allowed to vary within

Table 3: Summary of the event selection in each control region corresponding to b0L-SRA and b0L-SRB. The term lepton is used in the table to refer to baseline electrons and muons. Jets ( $j_1$ ,  $j_2$ ,  $j_3$  and  $j_4$ ) and leptons ( $\ell_1$  and  $\ell_2$ ) are labelled with an index corresponding to their decreasing order in  $p_T$ .

b0L-	CRzA	CRttA	CRstA	CRwA	CRzB	CRttB	CRwB
Number of leptons ( $\ell = e, \mu$ )	2 SFOS	1	1	1	2 SFOS	1	1
$p_T(\ell_1)$ [GeV]	> 90	> 27	> 27	> 27	> 27	> 27	> 27
$p_T(\ell_2)$ [GeV]	> 20	–	–	–	> 20	–	–
$m_{\ell\ell}$ [GeV]	[76–106]	–	–	–	[76–106]	–	–
$N_{\text{jets}}$ ( $p_T > 35$ GeV)	2–4	2–4	2–4	2–4	2–4	2–4	2–4
$p_T(j_1)$ [GeV]	> 50	> 130	–	> 130	> 50	> 50	> 50
$p_T(j_2)$ [GeV]	> 50	> 50	> 50	> 50	> 50	> 50	> 50
$p_T(j_4)$ [GeV]	< 50	< 50	< 50	< 50	–	–	–
$b$ -jets	$j_1$ and $j_2$	$j_1$ and $j_2$	$j_1$ and $j_2$	$j_1$	any 2	any 2	any 2
$E_T^{\text{miss}}$ [GeV]	< 100	> 200	> 200	> 200	< 100	> 100	> 100
$E_T^{\text{miss,cor}}$ [GeV]	> 100	–	–	–	> 200	–	–
$E_T^{\text{miss}}/m_{\text{eff}}$	> 0.25	> 0.25	> 0.25	> 0.25	–	–	–
$\min[\Delta\phi(\text{jet}_{1-4}, E_T^{\text{miss}})]$	–	> 0.4	> 0.4	> 0.4	> 0.4	> 0.4	> 0.4
$m_T$ [GeV]	–	–	–	> 30	–	> 30	> 30
$m_{bb}$ [GeV]	> 200	< 200	> 200	$m_{bj} > 200$	–	–	–
$m_{\text{CT}}$ [GeV]	> 250	> 250	> 250	> 250	–	–	–
$m_{b\ell}^{\text{min}}$ [GeV]	–	–	> 170	–	–	–	–
$m_T^{\text{min}}(\text{jet}_{1-4}, E_T^{\text{miss}})$ [GeV]	–	–	–	–	> 200	> 200	> 250
$\Delta\phi(b_1, E_T^{\text{miss}})$	–	–	–	–	–	< 2.0	< 2.0
$\Delta\phi(b_2, E_T^{\text{miss}})$	–	–	–	–	–	< 2.5	–

Table 4: Summary of the event selection in each control region corresponding to b0L-SRC. The term lepton is used in the table to refer to baseline electrons and muons. Jets ( $j_1$ ,  $j_2$ ,  $j_3$  and  $j_4$ ) and leptons ( $\ell_1$  and  $\ell_2$ ) are labelled with an index corresponding to their decreasing order in  $p_T$ .

b0L-	CRzC	CRttC	CRwC
Number of leptons ( $\ell = e, \mu$ )	2 SFOS	1	1
$p_T(\ell_1)$ [GeV]	> 27	> 27	> 27
$p_T(\ell_2)$ [GeV]	> 20	–	–
$m_{\ell\ell}$ [GeV]	[76–106]	–	–
$N_{\text{jets}}$ ( $p_T > 20$ GeV)	2–5	2–5	2–5
Leading jet $p_T$ [GeV]	> 250	> 500	> 500
$b$ -jets	$j_2$ and ( $j_3$ or $j_4$ )	$j_2$ and ( $j_3$ or $j_4$ )	$j_2$
$E_T^{\text{miss}}$ [GeV]	< 100	> 100	> 100
$E_T^{\text{miss,cor}}$ [GeV]	> 200	–	–
$m_T$ [GeV]	–	> 30	[30–120]
$m_{\text{eff}}$ [GeV]	> 500	> 1300	> 500
$m_{jj}$ [GeV]	> 200	> 200	> 200
$H_{\text{T4}}$ [GeV]	< 70	< 70	< 70
$\mathcal{A}$	> 0.5	> 0.5	> 0.8
$\Delta\phi(j_1, E_T^{\text{miss}})$	> 2.5	> 2.5	> 2.5

their normalisation uncertainty. The background from multijet production is estimated from data using a procedure described in detail in Ref. [78] and modified to account for the heavy flavour of the jets. The contribution from multijet production in all regions is found to be negligible.

In total four CRs are defined for the b0L-SRA to estimate  $W$ +jets,  $Z$ +jets,  $t\bar{t}$  and single top-quark production independently, while three CRs are defined for each of the b0L-SRB and b0L-SRC to estimate  $W$ +jets,  $Z$ +jets and  $t\bar{t}$ . The  $E_T^{\text{miss}}$  distribution in b0L-CRwA and b0L-CRzC is shown in Figure 2(a) and 2(b), where good agreement with the SM prediction is achieved after the background-only fit. The yields in all these CRs are shown in Figure 3 and compared to the MC predictions before the likelihood fit is performed, including only the statistical uncertainty on the MC samples. The bottom panel shows the value of the normalisation factors used for each of the backgrounds fitted.

As a further validation, two alternative methods are used to estimate the  $Z$ +jets contribution. The first method exploits the similarity of the  $Z$ +jets and  $\gamma$ +jets processes [78]. For a  $p_T$  of the photon significantly larger than the mass of the  $Z$  boson, the kinematics of  $\gamma$ +jets events strongly resemble those of  $Z$ +jets events. A set of dedicated control regions is defined by requesting one isolated photon with  $p_T > 145$  GeV. The  $p_T$  of the photon is vectorially added to the  $p_T^{\text{miss}}$ , and the magnitude of this sum replaces the  $E_T^{\text{miss}}$ -based selections. The yields are then propagated to the actual SRs using a reweighting factor derived using the MC simulation. This factor takes into account the different kinematics of the two processes and residual effects arising from the different geometrical acceptance and reconstruction efficiency for photons. In the second alternative method, applied to b0L-SRA only, the MC simulation is used to verify that the shape of the  $m_{\text{CT}}$  distribution for events with no  $b$ -tagged jets is compatible with the shape of the  $m_{\text{CT}}$  distribution for events where two  $b$ -tagged jets are present. A new highly populated  $Z$ +jets CR is defined selecting  $Z \rightarrow \ell\ell$  events with no  $b$ -tagged jets. The  $m_{\text{CT}}$  distribution in this CR is constructed using the two leading jets and is used to estimate the shape of the  $m_{\text{CT}}$  distribution in the b0L-SRA, whilst the normalization in SRA is rescaled based on the ratio in data of  $Z \rightarrow \ell\ell$  events with no  $b$ -tagged jets to events with two  $b$ -tagged jets. Additional MC-based corrections are applied to take into account the two-lepton selection in this CR. The two alternative methods are in agreement within uncertainties with the estimates obtained with the profile likelihood fit to the control regions. Experimental and theoretical systematic uncertainties in the nominal and alternative method estimates are taken into account (see Section 7). The difference between the alternative methods and the background-only fit is taken into account as an additional systematic uncertainty in the final  $Z$ +jets yields.

## 6.2 Background estimation in the one-lepton signal regions

The main SM background in the b1L signal regions is the production of  $t\bar{t}$  and single top-quark events in the  $Wt$  channel. Two control regions (b1L-CRttA and b1L-CRttB) where the  $t\bar{t}$  production is enhanced are defined by inverting the  $am_{\text{T2}}$  selection. In the case of b1L-CRttA the  $m_{bb}$  selection is also inverted, while for b1L-CRttB the  $\min[m_{\text{T}}(\text{bjet}, E_T^{\text{miss}})]$  requirement is inverted. To allow a statistical combination of the results from the b0L-SRA and b1L-SRA regions the corresponding  $t\bar{t}$  CRs are defined to be orthogonal via the  $m_{\text{CT}}$  selection. The single top-quark contribution is estimated with the same CR employed by the b0L analysis. In the case of b1L-SRB the production of  $W$ +jets is no longer negligible, and is studied by using a dedicated control region b1L-CRwB, where only one  $b$ -tagged jet is required. In total two CRs are used to estimate the event yields in b1L-SRA and three CRs to estimate the yields in b1L-SRB. Full details of the CR selections are given in Table 5. The distribution of  $m_{bb}$  in b1L-CRstA and of  $m_{\text{T}}$  in b1L-CRttB are presented in Figure 2(c) and 2(d) to show the agreement achieved after the background-only fit. The yields in all these CRs are also shown in Figure 3 and compared to the direct MC prediction before the likelihood

fit is performed. Within uncertainties, the normalisation parameters are generally consistent with unity. The decrease of the  $\mu_{t\bar{t}}$  parameter from SRA to SRC is related to mismodelling in the description of top-pair processes by POWHEG +PYTHIA 6 MC samples. Previous analyses [79] also found normalisation factors considerably smaller than unity for top-pair background processes in similarly extreme regions of phase space. The  $W$ +jets and  $Z$ +jets normalisation factors are larger than unity. This is possibly related to the fact that in the default SHERPA 2.2.1 the heavy-flavour production fractions are not consistent with the measured values [80].

Table 5: Summary of the event selection in each control region corresponding to the b1L signal regions. The term lepton is used in the table to refer to baseline electrons and muons. Jets ( $j_1$ ,  $j_2$ ,  $j_3$  and  $j_4$ ) and leptons ( $\ell_1$  and  $\ell_2$ ) are labelled with an index corresponding to their decreasing order in  $p_T$ .

b1L-	CRttA	CRstA	CRttB	CRstB	CRwB
Number of leptons ( $\ell = e, \mu$ )	1	1	1	1	1
$p_T(\ell_1)$ [GeV]	$> 27$	$> 27$	$> 27$	$> 27$	$> 27$
$N_{\text{jets}}$ ( $p_T > 35$ GeV)	$\geq 2$	[2–4]	$\geq 2$	$\geq 2$	$\geq 2$
$p_T(j_1)$ [GeV]	$> 35$	$> 130$	$> 35$	$> 35$	$> 35$
$p_T(j_2)$ [GeV]	$> 35$	$> 50$	$> 35$	$> 35$	$> 35$
$p_T(j_4)$ [GeV]	$> 35$	[35–50]	–	–	–
$\min[\Delta\phi(\text{jet}_{1-4}, E_T^{\text{miss}})]$	$> 0.4$	$> 0.4$	$> 0.4$	$> 0.4$	$> 0.4$
$b$ -jets	any 2	$j_1$ and ( $j_2$ or $j_3$ or $j_4$ )	any 2	any 2	any 1
$m_{bb}$ [GeV]	$< 200$	$> 200$	$< 200$	$> 200$	$> 200$
$m_{bl}^{\min}$ [GeV]	$< 170$	$> 170$	$< 170$	$> 170$	$< 170$
$E_T^{\text{miss}}$ [GeV]	$> 200$	$> 200$	$> 200$	$> 200$	$> 200$
$m_T$ [GeV]	$> 140$	–	$> 120$	[30–120]	[30–120]
$am_{T2}$ [GeV]	$< 250$	–	$< 200$	–	$> 200$
$m_{\text{eff}}$ [GeV]	$> 300$	–	–	–	–
$m_{CT}$ [GeV]	$< 250$	$> 250$	–	–	–
$E_T^{\text{miss}} / \sqrt{H_T}$ [GeV $^{1/2}$ ]	$> 8$	–	$> 8$	$> 8$	$> 8$
$E_T^{\text{miss}} / m_{\text{eff}}$	–	$> 0.25$	–	–	–
$m_T^{\min}(\text{bjet}_{1-2}, E_T^{\text{miss}})$ [GeV]	–	–	$< 200$	$> 200$	$> 200$
$\Delta\phi(b_1, E_T^{\text{miss}})$	–	–	$> 2.0$	$> 2.0$	$> 2.0$

### 6.3 Validation regions

The results of the background-only fit to the CRs, are extrapolated to a set of VRs defined to be similar to the SRs, with some of the selection criteria modified to enhance the background contribution, while maintaining a small signal contribution. For each SR one or more VRs are defined as:

- b0L-VRmctA. Same as b0L-SRA except:  $m_T^{\min}(\text{jet}_{1-4}, E_T^{\text{miss}}) < 250$  GeV,  $150 < m_{CT} < 250$  GeV;
- b0L-VRmbbA. Same as b0L-SRA except:  $m_T^{\min}(\text{jet}_{1-4}, E_T^{\text{miss}}) < 250$  GeV,  $100 < m_{bb} < 200$  GeV;
- b0L-VRzB. Same as b0L-SRB except:  $m_{CT} < 250$  GeV,  $200 < m_T^{\min}(\text{jet}_{1-4}, E_T^{\text{miss}}) < 250$  GeV,  $\mathcal{A} < 0.8$ , no selection on  $\Delta\phi(b_1, E_T^{\text{miss}})$  and  $\Delta\phi(b_2, E_T^{\text{miss}})$ ;
- b0L-VRttB. Same as b0L-SRB except:  $m_{CT} < 250$  GeV,  $150 < m_T^{\min}(\text{jet}_{1-4}, E_T^{\text{miss}}) < 200$  GeV,  $\mathcal{A} < 0.8$ ;

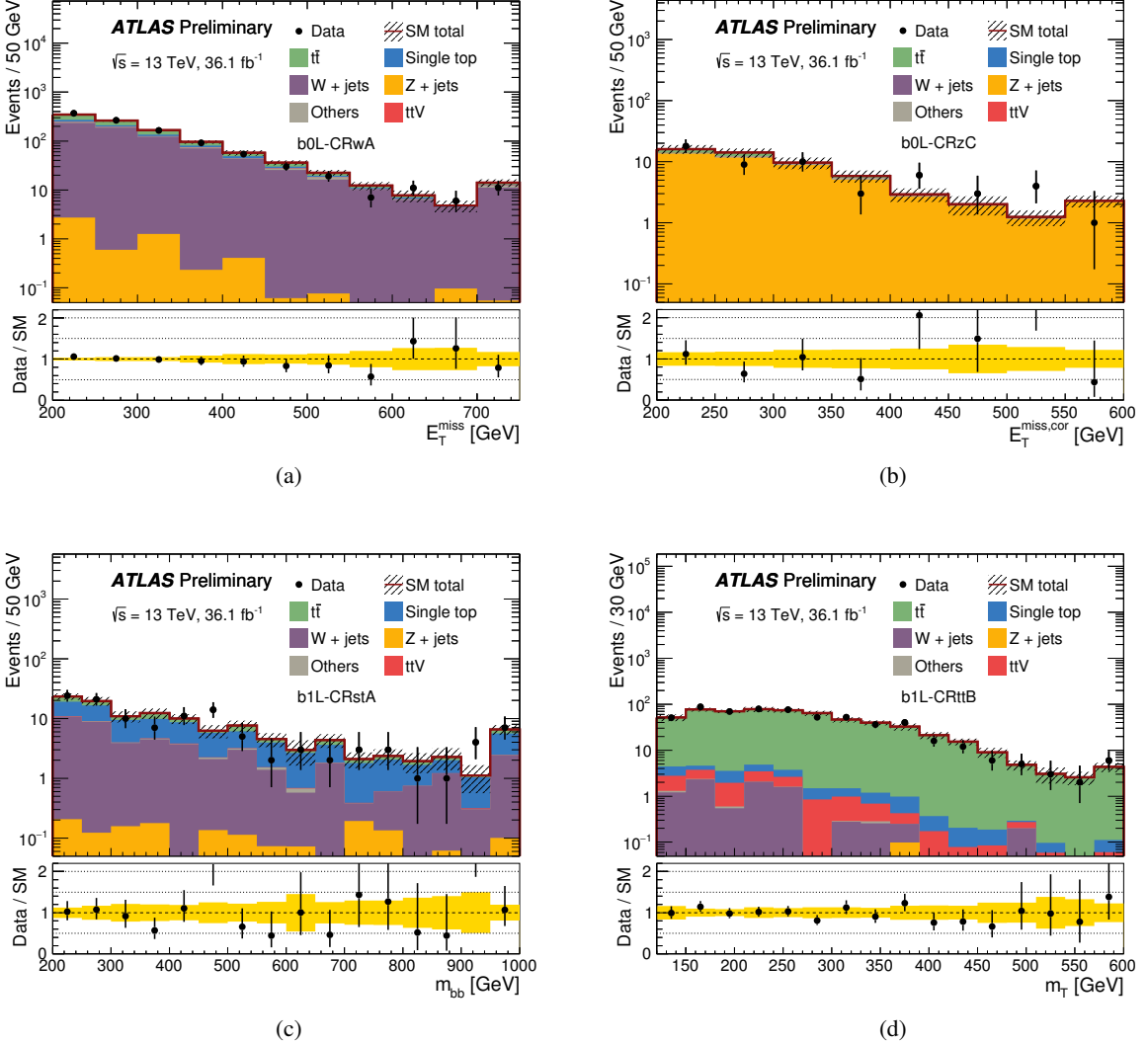


Figure 2: Example kinematic distributions in some of the control regions. (a)  $E_T^{\text{miss}}$  in b0L-CRwA, (b)  $E_T^{\text{miss,cor}}$  in b0L-CRzC, (c)  $m_{bb}$  in b1L-CRstA, (d)  $m_T$  in b1L-CRttB. In all distributions the MC normalization is rescaled using the results from the background-only fit, showing good agreement between data and the predicted SM shapes. The shaded-grey band in the top panel and the yellow band in the bottom panel show statistical and detector-related systematic uncertainties as detailed in Section 7 and the last bin includes overflows.

- b0L-VRttC. Same as b0L-SRC except:  $m_{CT} < 250 \text{ GeV}$ ,  $m_T^{\min}(\text{jet}_{1-4}, E_T^{\text{miss}}) < 250 \text{ GeV}$ ,  $0.6 < \mathcal{A} < 0.8$ ;
- b0L-VRqC. Same as b0L-SRC except:  $m_{CT} < 250 \text{ GeV}$ ,  $m_T^{\min}(\text{jet}_{1-4}, E_T^{\text{miss}}) < 250 \text{ GeV}$ ,  $200 < E_T^{\text{miss}} < 500 \text{ GeV}$ ,  $0.2 < \mathcal{A} < 0.8$ , no selection on  $\min[\Delta\phi(\text{jet}_{1-2}, E_T^{\text{miss}})]$ ;
- b1L-VRamt2A. Same as b1L-SRA300-2j except:  $30 < m_T < 140 \text{ GeV}$ ,  $m_{bb} < 200 \text{ GeV}$ ;
- b1L-VRmbbA. Same as b1L-SRA300-2j except:  $am_{T2} < 250 \text{ GeV}$ ;

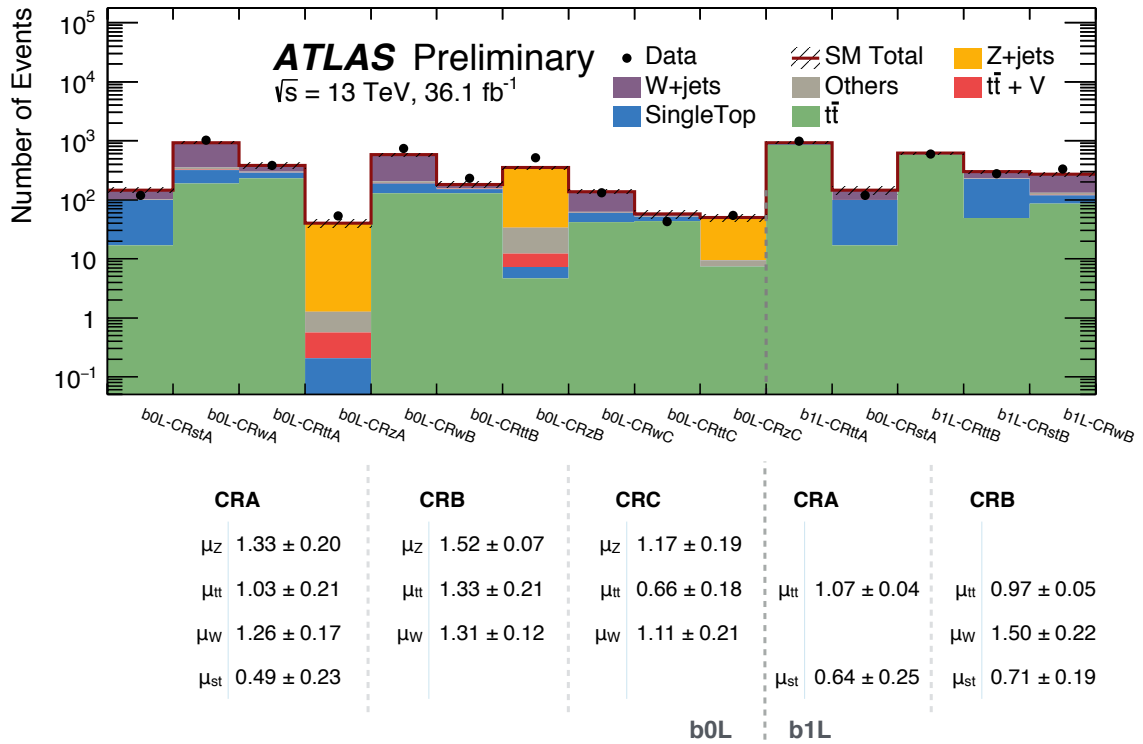


Figure 3: Results of the likelihood fit to the CRs associated to each of the b0L and b1L SRs. In the top panel the normalisation of the backgrounds is obtained from the Monte Carlo and is the input value to the fit. The panels at the bottom show the value of the normalisation factors ( $\mu$ ) obtained for each of the background fitted. The vertical dashed lines separate each set of CRs corresponding to each individual SR. The uncertainty band on the MC prediction includes only the statistical uncertainty on the MC samples.

- b1L-VRamt2B. Same as b1L-SRB except:  $\Delta\phi(b_1, E_T^{\text{miss}}) > 2.0$ ,  $m_{bb} > 200$  GeV;
- b1L-VRmbbB. Same as b1L-SRB except:  $\Delta\phi(b_1, E_T^{\text{miss}}) > 2.0$ ,  $30 < m_T < 120$  GeV;

The number of events predicted by the background-only fit is compared to the data in the upper panel of Figure 4. The pull, defined by the difference between the observed number of events ( $n_{\text{obs}}$ ) and the predicted background yield ( $n_{\text{pred}}$ ) divided by the total uncertainty ( $\sigma_{\text{tot}}$ ), is shown for each region in the lower panel. No evidence of significant background mis-modelling is observed in the VRs.

## 7 Systematic uncertainties

Several sources of experimental and theoretical systematic uncertainty in the signal and background estimates are considered in these analyses. Their impact is reduced through the normalization of the dominant backgrounds in the control regions defined with kinematic selections resembling those of the corresponding signal region (see Section 6). Experimental and theoretical uncertainties are included as nuisance parameters with Gaussian constraints in the likelihood fits, taking into account correlations. Uncertainties due to the number of events in the CRs are also introduced in the fit for each region. The dominant contributions are summarised in Table 6.

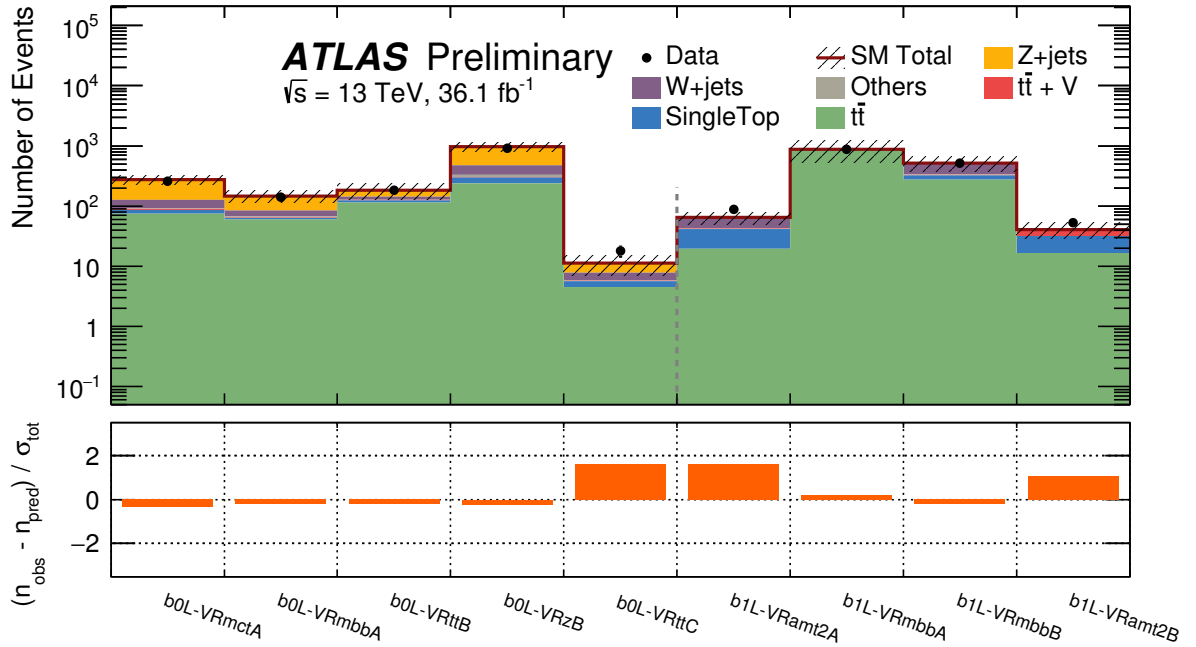


Figure 4: Results of the likelihood fit extrapolated to the VRs associated to the b0L and b1L analyses. The normalization of the backgrounds is obtained from the fit to the CRs. The upper panel shows the observed number of events and the predicted background yield. All uncertainties defined in Section 7 are included in the uncertainty band. The lower panel shows the pulls in each VR.

The dominant detector-related systematic effects are due to the uncertainties in the jet energy scale (JES) [58] and resolution (JER) [81], and in the  $b$ -tagging efficiency and mis-tagging rates. The latter are estimated by varying the  $\eta$ -,  $p_T$ - and flavour-dependent scale factors applied to each jet in the simulation within a range that reflects the systematic uncertainty on the measured tagging efficiency and mis-tag rates using 13 TeV data. The uncertainties associated with lepton and photon reconstruction and energy measurements are also considered but have a negligible impact on the final results. Lepton, photon and jet-related uncertainties are propagated to the calculation of the  $E_T^{\text{miss}}$ , and additional uncertainties are included in the energy scale and resolution of the soft term.

Uncertainties in the modelling of the SM background processes from MC simulation and their theoretical cross-section uncertainties are also taken into account. The dominant uncertainty arises from  $Z$ -jets MC modelling for b0L-SRs and  $t\bar{t}$  and single-top modelling (collectively referred to as “Top production” in Table 6) for b1L-SRs. The  $Z$ -jets (as well as  $W$ -jets) modelling uncertainties are evaluated considering different merging (CKKW-L) and resummation scales using alternative samples, PDF variations from the NNPDF30NNLO replicas [44], as well as an envelope formed from 7-point scale variations of the renormalisation and factorisation scales. The various components are added in quadrature. A 40% uncertainty [82] is assigned to the heavy-flavour jet content in  $W$ -jets, estimated from MC simulation in the one-lepton channel signal regions. For b0L-SRA, the uncertainty accounts for the different requirements on  $b$ -jets between CRAs and the signal regions.

Theoretical and modelling uncertainties of the top-quark pair and single-top-quark ( $Wt$ ) backgrounds are computed as the difference between the prediction from nominal samples and those of additional

Table 6: Summary of the dominant experimental and theoretical uncertainties for each signal region in zero-lepton and one-lepton channels. Uncertainties are quoted as relative to the total SM background predictions, with a range indicated for the three b0L-SRAs and the two b1L-SRAs. For theoretical modelling, uncertainties per dominant SM background process are quoted. The individual uncertainties can be correlated, and do not necessarily add in quadrature to the total background uncertainty.

Source \ Region	b0L-SRAx	b0L-SRB	b0L-SRC	b1L-SRAx	b1L-SRB	b1L-SRA300-2j
Experimental uncertainty						
JES	2.3-3.4%	5.7%	4.3%	1.2-1.5%	0.9%	6.9%
JER	0.9-3.3%	3.5%	10.6%	5.3-8.6%	0.9%	4%
<i>b</i> -tagging	3.3-4.3%	7.5%	4.7%	6.1-6.3%	2%	6.6%
Theoretical modelling uncertainty						
Z+jets	9.6-12.3%	13%	11.3%	-	-	-
W+jets	3.4-5.2%	4.7%	7.6%	1.3-1.6%	8.6%	7.9%
Top production	2.2-3.1%	6%	3.6%	18.6-18.7%	13.4%	22%

samples differing in generator or parameter settings. Hadronization and PS uncertainties are estimated using samples generated with PowHEG-Box v2 and showered by HERWIG++ v2.7.1 [83] with the UEEE5 underlying event tune. Uncertainties related to initial- and final-state radiation modelling, PS tune and (for  $t\bar{t}$  only) choice of  $h_{\text{damp}}$  parameter in PowHEG-Box v2 are evaluated using alternative settings of the generators. Finally, an alternative generator MADGRAPH5\_aMC@NLO with showering by HERWIG++ v2.7.1 is used to estimate the generator uncertainties. One additional uncertainty stems from the modelling of the interference between the  $t\bar{t}$  and  $Wt$  processes at NLO. Predictions from an inclusive  $WWbb$  sample generated at LO using MADGRAPH5\_aMC@NLO are compared with the sum of the  $t\bar{t}$  and  $Wt$  processes and differences with the nominal predictions are taken as systematic uncertainties.

Uncertainties in backgrounds such as diboson and  $t\bar{t}V$  are also estimated by comparisons of the nominal sample with alternative samples differing in generator or parameter settings (PowHEG v2 with showering by PYTHIA 8.210 for diboson, renormalization and factorization scale and A14 tune variations for  $t\bar{t}V$ ) and contribute less than 5% to the total uncertainty. The cross-sections used to normalize the MC yields to the highest order available are varied according to the scale uncertainty of the theoretical calculation. The cross-section uncertainties are 5% for  $W$ ,  $Z$  boson and top-quark pair production, 6% for diboson, 13% and 12% for  $t\bar{t}W$  and  $t\bar{t}Z$ , respectively. Finally, a conservative 100% systematic uncertainty associated to the multijet background estimate is considered and found to be negligible.

For the SUSY signal processes, both the experimental and theoretical uncertainties in the expected signal yield are considered. Experimental uncertainties are found to be between 15% and 30% across the  $\tilde{b}_1 - \tilde{\chi}_1^0$  mass plane for exclusive  $\tilde{b}_1 \rightarrow b\tilde{\chi}_1^0$  decays and between 10% and 25% for models where bottom squarks decay with significant branching ratio as  $\tilde{b}_1 \rightarrow t\tilde{\chi}_1^\pm$ , assuming one-lepton channel selection. In all SRs, they are largely dominated by the uncertainty in the *b*-tagging efficiency. Theoretical uncertainties in the NLO+NLL cross-section are calculated for each SUSY signal scenario and are dominated by the uncertainties in the renormalization and factorization scales, followed by the uncertainty in the PDF. They vary between 15% and 25% for bottom-squark masses in the range between 400 GeV and 1100 GeV. Additional uncertainties on the acceptance and efficiency due to the modelling of initial-state radiation and scale variations in SUSY signal MC samples are also taken into account and contribute up to about 10%.

Table 7: Fit results in the b0L signal regions for an integrated luminosity of  $36.1 \text{ fb}^{-1}$ . The background normalization parameters are obtained from the fit in the control regions and are applied to the SRs. Smaller backgrounds as diboson,  $t\bar{t}V$ , multijet and rare processes are indicated as “Others”. The individual uncertainties, including statistical, detector-related and theoretical systematic components, are symmetrized and can be correlated and do not necessarily add in quadrature to the total systematic uncertainty.

<b>b0L- Signal Region</b>	SRA350	SRA450	SRA550	SRB	SRC
Observed	81	24	10	45	7
Total background (fit)	$70 \pm 13$	$22 \pm 5$	$7.2 \pm 1.5$	$37 \pm 7$	$5.5 \pm 1.5$
$Z + \text{jets}$	$46 \pm 12$	$13.6 \pm 3.7$	$4.0 \pm 1.2$	$20.0 \pm 5.2$	$2.3 \pm 0.8$
$t\bar{t}$	$2.0 \pm 0.6$	$0.5 \pm 0.2$	$0.16 \pm 0.07$	$5.1 \pm 2.7$	$0.8 \pm 0.3$
Single top	$4.7 \pm 3.4$	$1.2 \pm 1.0$	$0.5 \pm 0.3$	$2.6 \pm 1.1$	$0.7 \pm 0.3$
$W + \text{jets}$	$15 \pm 5$	$5.0 \pm 1.8$	$2.4 \pm 1.0$	$5.5 \pm 2.0$	$1.3 \pm 0.8$
“Others”	$2.5 \pm 1.7$	$1.4 \pm 1.2$	$0.07 \pm 0.03$	$4.0 \pm 1.1$	$0.4 \pm 0.1$
Total background (MC exp.)	60.4	18.5	6.2	28	5.4
$Z + \text{jets}$	34.9	10.3	3.0	13.1	1.9
$t\bar{t}$	1.9	0.45	0.16	3.8	1.2
Single top	10	2.5	1.0	2.6	0.7
$W + \text{jets}$	11.6	4.0	1.9	4.2	1.2
“Others”	2.5	1.3	0.07	4.0	0.4

## 8 Results and interpretation

Tables 7 and 8 report the observed number of events and the SM prediction after the background-only fit for each signal region in the zero-lepton and one-lepton channel, respectively. The background-only fit results are compared to the pre-fit predictions based on MC simulation. The largest background contribution in b0L-SRs arises from  $Z \rightarrow \nu\bar{\nu}$  produced in association with  $b$ -quarks followed by  $W + \text{jets}$  production, whilst top-quark and  $W + \text{jets}$  production dominates SM predictions for b1L-SRs. The results are also summarised in Figure 5, where the pulls for each of the SRs are also presented. No excess above the expected Standard Model background yield is observed, although b1L-SRA300-2j presents a discrepancy between data and SM predictions of about  $1.5\sigma$ .

Figures 6 and 7 show the comparison between the observed data and the SM predictions for some relevant kinematic distributions for the b0L and b1L selections, respectively.

The results are translated into upper limits on contributions from physics beyond the SM (BSM) for each signal region. The  $\text{CL}_s$  method [84, 85] is used to derive the confidence level of the exclusion; signal models with a  $\text{CL}_s$  value below 0.05 are said to be excluded at 95% CL. The profile-likelihood-ratio test statistic is used to exclude the signal-plus-background hypothesis for specific signal models. When normalized by the integrated luminosity of the data sample, results can be interpreted as corresponding upper limits on the visible cross-section,  $\sigma_{\text{vis}}$ , defined as the product of the BSM production cross-section, the acceptance and the selection efficiency of a BSM signal. Table 9 summarizes the observed ( $S_{\text{obs}}^{95}$ ) and expected ( $S_{\text{exp}}^{95}$ ) 95% CL upper limits on the number of BSM events and on  $\sigma_{\text{vis}}$ . The  $p_0$ -values, which represent the probability of the SM background alone to fluctuate to the observed number of events or higher, are also provided.

Table 8: Fit results in the b1L signal regions for an integrated luminosity of  $36.1 \text{ fb}^{-1}$ . The background normalization parameters are obtained from the background-only fit in the control regions and are applied to the SRs. The background normalization parameters obtained with the background-only fit are applied to the SRs. Smaller backgrounds as diboson,  $Z+jets$ , multijet and rare processes are indicated as “Others”. The individual uncertainties, including detector-related and theoretical systematic components, are symmetrized and can be correlated and do not necessarily add in quadrature to the total systematic uncertainty.

<b>b1L- Signal Region</b>	SRA600	SRA750	SRB	SRA300-2j
Observed	21	13	69	12
Total background (fit)	$24 \pm 6$	$15 \pm 4$	$53 \pm 12$	$6.7 \pm 2.3$
$t\bar{t}$	$10 \pm 5$	$5.5 \pm 2.7$	$16 \pm 7$	$2.4 \pm 1.3$
Single top	$7 \pm 4$	$4.5 \pm 2.8$	$10 \pm 5$	$3.3 \pm 2.0$
$W+jets$	$0.9 \pm 0.5$	$0.6 \pm 0.3$	$17 \pm 8$	$0.4 \pm 0.3$
$t\bar{t}V$	$5.4 \pm 0.6$	$4.0 \pm 0.5$	$9 \pm 1$	$0.6 \pm 0.1$
“Others”	$0.07 \pm 0.02$	$0.07 \pm 0.03$	$1.8 \pm 0.3$	$0.07 \pm 0.02$
Total background (MC exp.)	27	17	52	8.4
$t\bar{t}$	9	5.1	16	2.2
Single top	11	7.1	14	5.2
$W+jets$	0.9	0.6	11	0.4
$t\bar{t}V$	5.4	4.0	9	0.6
“Others”	0.07	0.07	1.8	0.07

Table 9: Left to right: 95% CL upper limits on the visible cross-section ( $\langle \epsilon A \sigma \rangle_{\text{obs}}^{95}$ ) and on the number of signal events ( $S_{\text{obs}}^{95}$ ). The third column ( $S_{\text{exp}}^{95}$ ) shows the 95% CL upper limit on the number of signal events, given the expected number (and  $\pm 1\sigma$  variations of the expectation) of background events. The last column reports the  $p_0$ -values and  $Z$  (the number of equivalent Gaussian standard deviations). The maximum allowed  $p_0$ -value is truncated at 0.5.

<b>Signal channel</b>	$\langle \epsilon A \sigma \rangle_{\text{obs}}^{95} [\text{fb}]$	$S_{\text{obs}}^{95}$	$S_{\text{exp}}^{95}$	$p_0(Z)$
b0L-SRA350	1.06	38.2	$30.9^{+11.3}_{-8.4}$	0.28 (0.60)
b0L-SRA450	0.43	15.6	$13.9^{+5.6}_{-3.8}$	0.37 (0.34)
b0L-SRA550	0.30	10.7	$7.8^{+3.7}_{-1.6}$	0.20 (0.85)
b0L-SRB	0.72	26.1	$19.9^{+8.3}_{-5.4}$	0.23 (0.74)
b0L-SRC	0.24	8.7	$6.8^{+3.3}_{-1.3}$	0.30 (0.54)
b1L-SRA300-2j	0.39	14.1	$9.3^{+3.5}_{-3.1}$	0.08 (1.43)
b1L-SRA600	0.38	13.6	$14.8^{+5.4}_{-4.4}$	0.50 (0.00)
b1L-SRA750	0.27	9.9	$11.2^{+4.0}_{-2.3}$	0.50 (0.00)
b1L-SRB	1.12	40.3	$28.7^{+10.7}_{-8.2}$	0.21 (0.80)

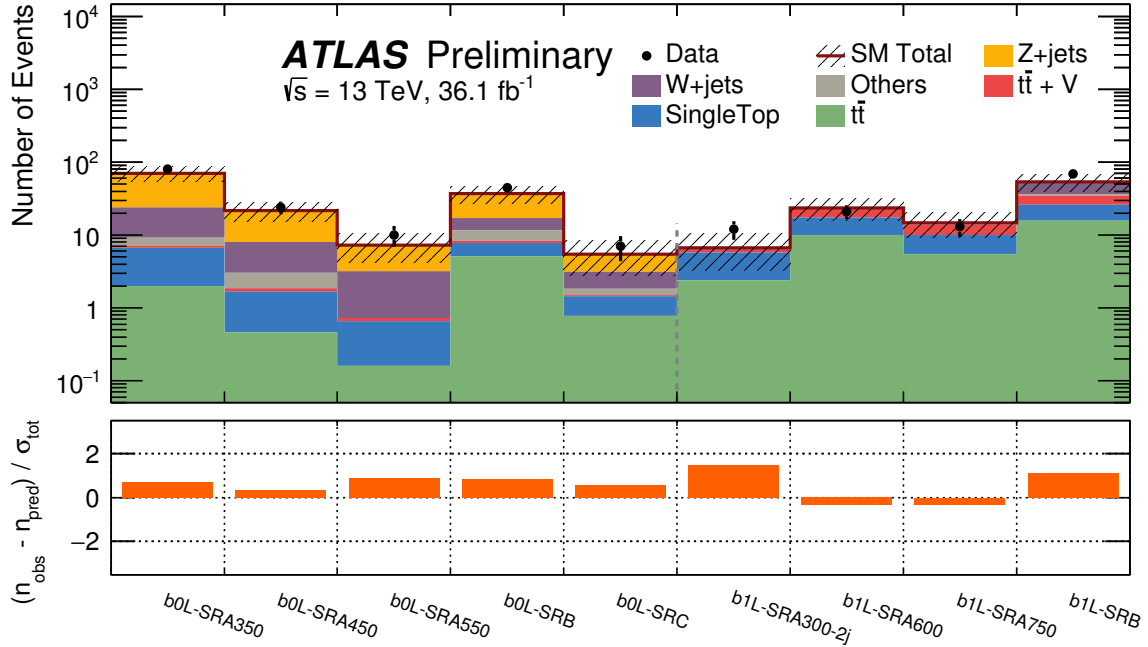


Figure 5: Results of the likelihood fit extrapolated to the SRs associated to the b0L and b1L analyses. The normalization of the backgrounds is obtained from the fit to the CRs. The upper panel shows the observed number of events and the predicted background yields. All uncertainties defined in Section 7 are included in the uncertainty band. The lower panel shows the pulls in each SR.

Exclusion limits are obtained assuming two types of SUSY particle mass hierarchy such that the lightest bottom squark decays either exclusively via  $\tilde{b}_1 \rightarrow b\tilde{\chi}_1^0$  or into multiple channels,  $\tilde{b}_1 \rightarrow b\tilde{\chi}_1^0$  and  $\tilde{b}_1 \rightarrow t\tilde{\chi}_1^\pm$ , assuming a 50% branching ratio and  $\Delta m(\tilde{\chi}_1^\pm, \tilde{\chi}_1^0) \sim 1$  GeV. The first set of scenarios is targeted by the zero-lepton channel SRs only. For models with mixed decays the best expected of b1L-SRAs is statistically combined either with the best expected of b1L-SRAs or with b1L-SRB. In all cases, the fit procedure takes into account correlations in the yield predictions between control and signal regions due to common background normalization parameters and systematic uncertainties. The experimental systematic uncertainties in the signal are taken into account for this calculation and are assumed to be fully correlated with those in the SM background.

For the exclusive  $\tilde{b}_1 \rightarrow b\tilde{\chi}_1^0$  decay mode, at each point of the parameter space the SR with the best expected sensitivity is used. Sensitivity to scenarios with the largest mass difference between the  $\tilde{b}_1$  and the  $\tilde{\chi}_1^0$  is achieved with the most stringent  $m_{\text{CT}}$  threshold (b0L-SRA550). Sensitivity to scenarios with intermediate and small mass differences is obtained with the dedicated b0L-SRB and b0L-SRC selections, respectively. For the mixed-decays scenarios, a statistical combination is computed with the results of b0L-SRAs and b1L-SRAs or b1L-SRB. A combined fit is performed simultaneously on the control and signal regions of the two analyses. The best sensitivity to regions of the  $(\tilde{b}_1, \tilde{\chi}_1^0)$  mass plane close to the kinematic boundaries is obtained with the combination of the b0L-SR450 and b1L-SRB regions whilst stringent constraints on large mass difference models are achieved with the results from the combination of zero-lepton and one-lepton SRs with the most stringent  $m_{\text{CT}}$  and  $m_{\text{eff}}$  thresholds, respectively.

Figures 8(a) and 8(b) show the observed (solid line) and expected (dashed line) exclusion contours at

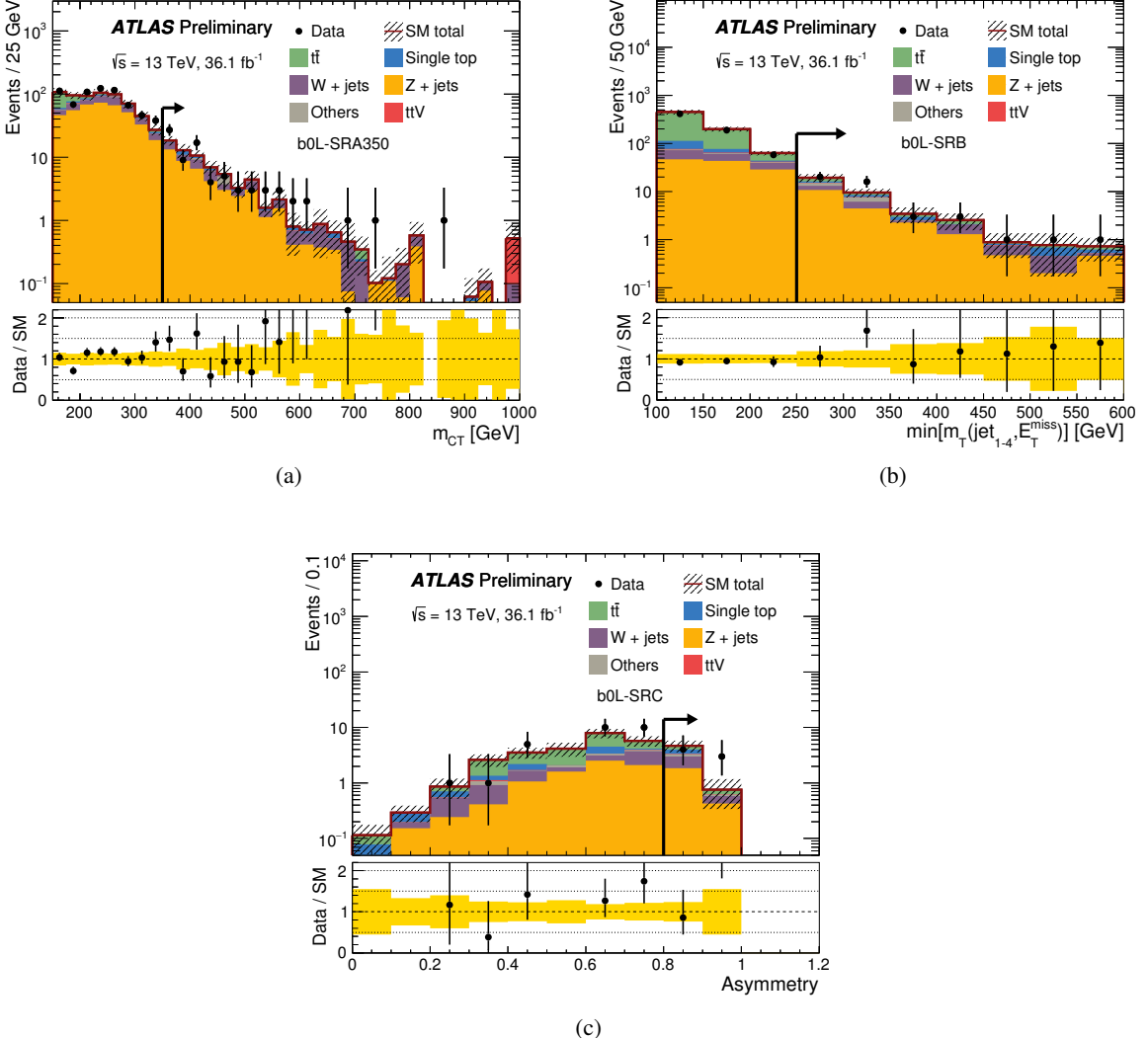


Figure 6: (a)  $m_{CT}$  distribution in b0L-SRA. (b)  $\min[m_T(\text{jet}_{1-4}, E_T^{\text{miss}})]$  distribution in b0L-SRB. (c)  $\mathcal{A}$  distribution in b0L-SRC. All selection criteria are applied, except the selection on the variable that is displayed in each of the plots. The arrows indicate the final selection applied in the signal regions. The shaded-grey band in the top panel and the yellow band in the bottom panel show statistical and detector-related systematic uncertainties. The SM backgrounds are normalized to the values determined in the fit. The last bin includes overflows.

95% CL in the  $\tilde{b}_1$ - $\tilde{\chi}_1^0$  mass plane for the two types of SUSY scenarios considered. Bottom-squark masses up to 950 (860) GeV are excluded for  $\tilde{\chi}_1^0$  masses below 420 (250) GeV in models with exclusive (mixed) decay modes. Multiple-decay bottom-squark models are phenomenologically equivalent to models characterized by the pair production of top squarks decaying as  $\tilde{t}_1 \rightarrow t\tilde{\chi}_1^0$  and  $\tilde{t}_1 \rightarrow b\tilde{\chi}_1^\pm$ , under the same assumptions for branching ratio and  $\Delta m(\tilde{\chi}_1^\pm, \tilde{\chi}_1^0)$ . Hence the results can be interpreted as exclusion limits on top-squark masses.

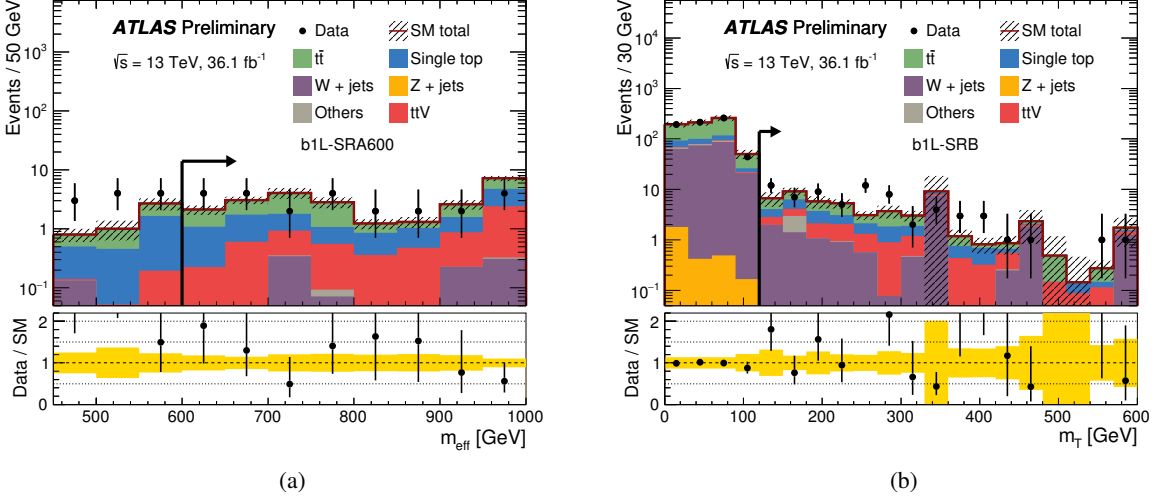


Figure 7: (a)  $m_{\text{eff}}$  distribution in b1L-SRA. (b)  $m_T$  distribution in b1L-SRB. All selection criteria are applied, except the selection on the variable that is displayed in each of the plots. The arrows indicate the final selection applied in the signal regions. The shaded-grey band in the top panel and the yellow band in the bottom panel show statistical and detector-related systematic uncertainties. The SM backgrounds are normalized to the values determined in the fit. The last bin includes overflows.

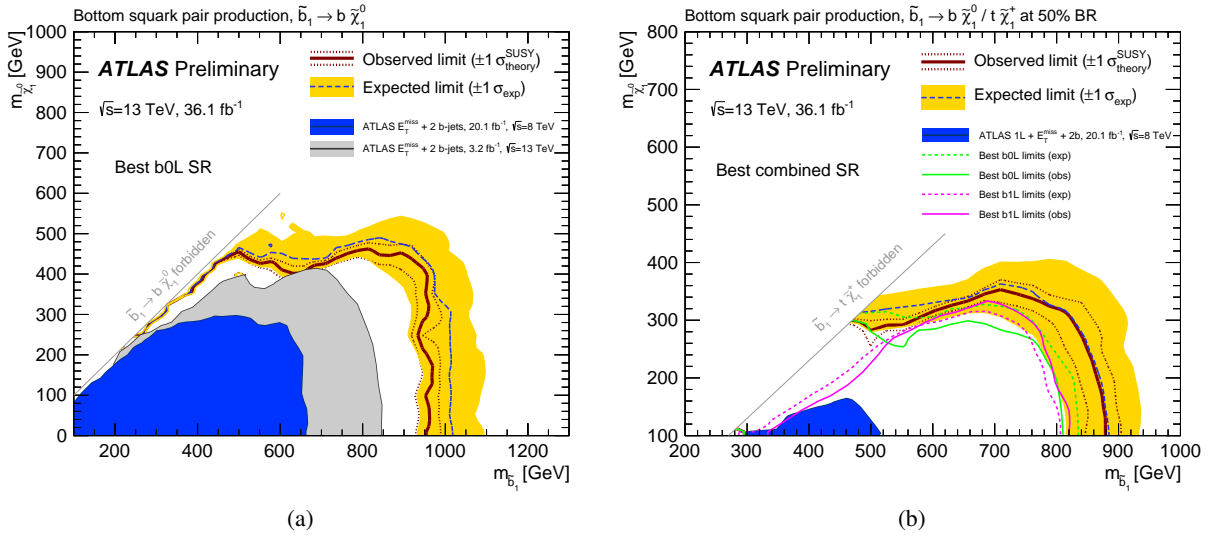


Figure 8: (a) Observed and expected exclusion contours at 95% CL, as well as  $\pm 1\sigma$  variation of the expected limit, in the  $\tilde{b}_1$ - $\tilde{\chi}_1^0$  mass plane. The SR with the best expected sensitivity is adopted for each point of the parameter space. The yellow band around the expected limit (dashed line) shows the impact of the experimental and SM background theoretical uncertainties. The dotted lines show the impact on the observed limit of the variation of the nominal signal cross-section by  $\pm 1\sigma$  of its theoretical uncertainties. (b) Same, for scenarios where multiple decay modes are considered for bottom squarks. The statistical combination of b0L-SRs and b1L-SRs is used in this case.

## 9 Conclusion

The results of a search for pair production of bottom and top squarks are reported. The analysis uses  $36.1 \text{ fb}^{-1}$  of  $pp$  collisions at  $\sqrt{s} = 13 \text{ TeV}$  collected by the ATLAS experiment at the Large Hadron Collider in 2015 and 2016. Third generation squarks are searched for in events containing large missing transverse momentum and jets, exactly two of which are identified as  $b$ -jets. Selections are defined with either no charged leptons (electrons and muons) in the final state, or one charged lepton. Zero-lepton channel signal regions target  $R$ -parity-conserving models in which the  $\tilde{b}_1$  is the lightest squark and is assumed to decay exclusively via  $\tilde{b}_1 \rightarrow b\tilde{\chi}_1^0$ , where  $\tilde{\chi}_1^0$  is the lightest neutralino. One-lepton channel signal regions target models where bottom or top squarks are produced and can decay into multiple channels,  $\tilde{b}_1 \rightarrow b\tilde{\chi}_1^0$  and  $\tilde{b}_1 \rightarrow t\tilde{\chi}_1^\pm$ , or  $\tilde{t}_1 \rightarrow t\tilde{\chi}_1^0$  and  $\tilde{t}_1 \rightarrow b\tilde{\chi}_1^\pm$ , where  $\tilde{\chi}_1^\pm$  is the lightest chargino and the mass difference  $m_{\tilde{\chi}_1^\pm} - m_{\tilde{\chi}_1^0}$  is set to 1 GeV. No excess above the expected Standard Model background is found and exclusion limits at 95% confidence level are placed on the visible cross-section and on the mass of the bottom (or top) squark. Bottom-squark masses up to 950 GeV are excluded for  $\tilde{\chi}_1^0$  masses below 420 GeV in models with exclusive decay modes. Bottom- or top- squark masses up to 860 GeV are excluded for  $\tilde{\chi}_1^0$  masses below 250 GeV in models with mixed decay modes with equal branching ratio. The results significantly extend the constraints on bottom-squark masses with respect to previous Run-1 and Run-2 searches at the ATLAS experiment.

## Acknowledgements

We thank CERN for the very successful operation of the LHC, as well as the support staff from our institutions without whom ATLAS could not be operated efficiently.

We acknowledge the support of ANPCyT, Argentina; YerPhI, Armenia; ARC, Australia; BMWFW and FWF, Austria; ANAS, Azerbaijan; SSTC, Belarus; CNPq and FAPESP, Brazil; NSERC, NRC and CFI, Canada; CERN; CONICYT, Chile; CAS, MOST and NSFC, China; COLCIENCIAS, Colombia; MSMT CR, MPO CR and VSC CR, Czech Republic; DNRF and DNSRC, Denmark; IN2P3-CNRS, CEA-DSM/IRFU, France; SRNSF, Georgia; BMBF, HGF, and MPG, Germany; GSRT, Greece; RGC, Hong Kong SAR, China; ISF, I-CORE and Benoziyo Center, Israel; INFN, Italy; MEXT and JSPS, Japan; CNRST, Morocco; NWO, Netherlands; RCN, Norway; MNiSW and NCN, Poland; FCT, Portugal; MNE/IFA, Romania; MES of Russia and NRC KI, Russian Federation; JINR; MESTD, Serbia; MSSR, Slovakia; ARRS and MIZŠ, Slovenia; DST/NRF, South Africa; MINECO, Spain; SRC and Wallenberg Foundation, Sweden; SERI, SNSF and Cantons of Bern and Geneva, Switzerland; MOST, Taiwan; TAEK, Turkey; STFC, United Kingdom; DOE and NSF, United States of America. In addition, individual groups and members have received support from BCKDF, the Canada Council, CANARIE, CRC, Compute Canada, FQRNT, and the Ontario Innovation Trust, Canada; EPLANET, ERC, ERDF, FP7, Horizon 2020 and Marie Skłodowska-Curie Actions, European Union; Investissements d’Avenir Labex and Idex, ANR, Région Auvergne and Fondation Partager le Savoir, France; DFG and AvH Foundation, Germany; Herakleitos, Thales and Aristea programmes co-financed by EU-ESF and the Greek NSRF; BSF, GIF and Minerva, Israel; BRF, Norway; CERCA Programme Generalitat de Catalunya, Generalitat Valenciana, Spain; the Royal Society and Leverhulme Trust, United Kingdom.

The crucial computing support from all WLCG partners is acknowledged gratefully, in particular from CERN, the ATLAS Tier-1 facilities at TRIUMF (Canada), NDGF (Denmark, Norway, Sweden), CC-IN2P3 (France), KIT/GridKA (Germany), INFN-CNAF (Italy), NL-T1 (Netherlands), PIC (Spain), ASGC

(Taiwan), RAL (UK) and BNL (USA), the Tier-2 facilities worldwide and large non-WLCG resource providers. Major contributors of computing resources are listed in Ref. [86].

## References

- [1] Yu. A. Golfand and E. P. Likhtman, *Extension of the Algebra of Poincare Group Generators and Violation of  $p$  Invariance*, JETP Lett. **13** (1971) 323–326, [Pisma Zh. Eksp. Teor. Fiz. 13, 452 (1971)].
- [2] D. V. Volkov and V. P. Akulov, *Is the Neutrino a Goldstone Particle?*, Phys. Lett. B **46** (1973) 109–110.
- [3] J. Wess and B. Zumino, *Supergauge Transformations in Four-Dimensions*, Nucl. Phys. B **70** (1974) 39–50.
- [4] J. Wess and B. Zumino, *Supergauge Invariant Extension of Quantum Electrodynamics*, Nucl. Phys. B **78** (1974) 1.
- [5] S. Ferrara and B. Zumino, *Supergauge Invariant Yang-Mills Theories*, Nucl. Phys. B **79** (1974) 413.
- [6] A. Salam and J. A. Strathdee, *Supersymmetry and Nonabelian Gauges*, Phys. Lett. B **51** (1974) 353–355.
- [7] N. Sakai, *Naturalness in Supersymmetric Guts*, Z. Phys. C **11** (1981) 153.
- [8] S. Dimopoulos, S. Raby, and F. Wilczek, *Supersymmetry and the Scale of Unification*, Phys. Rev. D **24** (1981) 1681–1683.
- [9] L. E. Ibanez and G. G. Ross, *Low-Energy Predictions in Supersymmetric Grand Unified Theories*, Phys. Lett. B **105** (1981) 439.
- [10] S. Dimopoulos and H. Georgi, *Softly Broken Supersymmetry and  $SU(5)$* , Nucl. Phys. B **193** (1981) 150.
- [11] H. Goldberg, *Constraint on the Photino Mass from Cosmology*, Phys. Rev. Lett. **50** (1983) 1419, [Erratum: Phys. Rev. Lett. 103, 099905 (2009)].
- [12] J. R. Ellis, J. S. Hagelin, D. V. Nanopoulos, K. A. Olive, and M. Srednicki, *Supersymmetric Relics from the Big Bang*, Nucl. Phys. B **238** (1984) 453–476.
- [13] R. Barbieri and G. F. Giudice, *Upper Bounds on Supersymmetric Particle Masses*, Nucl. Phys. B **306** (1988) 63.
- [14] B. de Carlos and J. A. Casas, *One loop analysis of the electroweak breaking in supersymmetric models and the fine tuning problem*, Phys. Lett. B **309** (1993) 320–328, [arXiv:hep-ph/9303291 \[hep-ph\]](https://arxiv.org/abs/hep-ph/9303291).
- [15] P. Fayet, *Supersymmetry and Weak, Electromagnetic and Strong Interactions*, Phys. Lett. B **64** (1976) 159.
- [16] P. Fayet, *Spontaneously Broken Supersymmetric Theories of Weak, Electromagnetic and Strong Interactions*, Phys. Lett. B **69** (1977) 489.

[17] G. R. Farrar and P. Fayet, *Phenomenology of the Production, Decay, and Detection of New Hadronic States Associated with Supersymmetry*, *Phys. Lett. B* **76** (1978) 575–579.

[18] ATLAS Collaboration, *Search for bottom squark pair production in proton–proton collisions at  $\sqrt{s} = 13$  TeV with the ATLAS detector*, *Eur. Phys. J. C* **76** (2016) 547, [arXiv:1606.08772 \[hep-ex\]](https://arxiv.org/abs/1606.08772).

[19] CMS Collaboration, *Search for supersymmetry in multijet events with missing transverse momentum in proton-proton collisions at 13 TeV*, [arXiv:1704.07781 \[hep-ex\]](https://arxiv.org/abs/1704.07781).

[20] ATLAS Collaboration, *ATLAS Run 1 searches for direct pair production of third-generation squarks at the Large Hadron Collider*, *Eur. Phys. J. C* **75** (2015) 510, [arXiv:1506.08616 \[hep-ex\]](https://arxiv.org/abs/1506.08616).

[21] ATLAS Collaboration, *The ATLAS Experiment at the CERN Large Hadron Collider*, *JINST* **3** (2008) S08003.

[22] ATLAS Collaboration, *ATLAS Insertable B-Layer Technical Design Report*, ATLAS-TDR-19, 2010, [http://cds.cern.ch/record/1291633](https://cds.cern.ch/record/1291633), Addendum: ATLAS-TDR-19-ADD-1, 2012, [http://cds.cern.ch/record/1451888](https://cds.cern.ch/record/1451888).

[23] ATLAS Collaboration, *Performance of the ATLAS Trigger System in 2010*, *Eur. Phys. J. C* **72** (2012) 1849, [arXiv:1110.1530 \[hep-ex\]](https://arxiv.org/abs/1110.1530).

[24] ATLAS Collaboration, *Improved luminosity determination in  $pp$  collisions at  $\sqrt{s} = 7$  TeV using the ATLAS detector at the LHC*, *Eur. Phys. J. C* **73** (2013) 2518, [arXiv:1302.4393 \[hep-ex\]](https://arxiv.org/abs/1302.4393).

[25] ATLAS Collaboration, *2015 start-up trigger menu and initial performance assessment of the ATLAS trigger using Run-2 data*, ATL-DAQ-PUB-2016-001, 2016, <https://cds.cern.ch/record/2136007/>.

[26] S. Agostinelli et al. (GEANT4), *GEANT4: A simulation toolkit*, *Nucl. Instrum. Meth. A* **506** (2003) 250.

[27] ATLAS Collaboration, *The ATLAS Simulation Infrastructure*, *Eur. Phys. J. C* **70** (2010) 823, [arXiv:1005.4568 \[hep-ex\]](https://arxiv.org/abs/1005.4568).

[28] J. Alwall et al., *The automated computation of tree-level and next-to-leading order differential cross sections, and their matching to parton shower simulations*, *JHEP* **1407** (2014) 079, [arXiv:1405.0301 \[hep-ph\]](https://arxiv.org/abs/1405.0301).

[29] T. Sjostrand, S. Mrenna, and P. Z. Skands, *A Brief Introduction to PYTHIA 8.1*, *Comput. Phys. Commun.* **178** (2008) 852, [arXiv:0710.3820 \[hep-ph\]](https://arxiv.org/abs/0710.3820).

[30] ATLAS Collaboration, *ATLAS Pythia 8 tunes to 7 TeV data*, ATL-PHYS-PUB-2014-021, 2014, <https://cds.cern.ch/record/1966419>.

[31] L. Lönnblad and S. Prestel, *Merging Multi-leg NLO Matrix Elements with Parton Showers*, *JHEP* **1303** (2013) 166, [arXiv:1211.7278 \[hep-ph\]](https://arxiv.org/abs/1211.7278).

[32] R. D. Ball et al., *Parton distributions with LHC data*, *Nucl. Phys. B* **867** (2013) 244, [arXiv:1207.1303 \[hep-ph\]](https://arxiv.org/abs/1207.1303).

[33] W. Beenakker, M. Kramer, T. Plehn, M. Spira, and P. M. Zerwas, *Stop production at hadron colliders*, *Nucl. Phys.* **B515** (1998) 3–14, [hep-ph/9710451](https://arxiv.org/abs/hep-ph/9710451).

[34] W. Beenakker, S. Brensing, M. Kramer, A. Kulesza, E. Laenen, and I. Niessen, *Supersymmetric top and bottom squark production at hadron colliders*, JHEP **1008** (2010) 098, [arXiv:1006.4771](https://arxiv.org/abs/1006.4771) [hep-ph].

[35] W. Beenakker et al., *Squark and gluino hadroproduction*, Int.J.Mod.Phys. **A26** (2011) 2637–2664, [arXiv:1105.1110](https://arxiv.org/abs/1105.1110) [hep-ph].

[36] C. Borschensky, M. Kramer, A. Kulesza, M. Mangano, S. Padhi, T. Plehn, and X. Portell, *Squark and gluino production cross sections in  $pp$  collisions at  $\sqrt{s} = 13, 14, 33$  and  $100$  TeV*, Eur. Phys. J. **C 74** (2014) 3174, [arXiv:1407.5066](https://arxiv.org/abs/1407.5066) [hep-ph].

[37] S. Alioli, P. Nason, C. Oleari, and E. Re, *A general framework for implementing NLO calculations in shower Monte Carlo programs: the POWHEG BOX*, JHEP **1006** (2010) 043, [arXiv:1002.2581](https://arxiv.org/abs/1002.2581) [hep-ph].

[38] H.-L. Lai, M. Guzzi, J. Huston, Z. Li, P. M. Nadolsky, J. Pumplin, and C. P. Yuan, *New parton distributions for collider physics*, Phys. Rev. **D82** (2010) 074024, [arXiv:1007.2241](https://arxiv.org/abs/1007.2241) [hep-ph].

[39] T. Sjostrand, S. Mrenna, and P. Z. Skands, *PYTHIA 6.4 Physics and Manual*, JHEP **0605** (2006) 026, [arXiv:hep-ph/0603175](https://arxiv.org/abs/hep-ph/0603175).

[40] M. Czakon and A. Mitov, *Top++: A Program for the Calculation of the Top-Pair Cross-Section at Hadron Colliders*, Comput. Phys. Commun. **185** (2014) 2930, [arXiv:1112.5675](https://arxiv.org/abs/1112.5675) [hep-ph].

[41] N. Kidonakis, *Next-to-next-to-leading-order collinear and soft gluon corrections for  $t$ -channel single top quark production*, Phys. Rev. D **83** (2011) 091503, [arXiv:1103.2792](https://arxiv.org/abs/1103.2792) [hep-ph].

[42] N. Kidonakis, *NNLL resummation for  $s$ -channel single top quark production*, Phys. Rev. D **81** (2010) 054028, [arXiv:1001.5034](https://arxiv.org/abs/1001.5034) [hep-ph].

[43] N. Kidonakis, *Two-loop soft anomalous dimensions for single top quark associated production with a  $W$ - or  $H$ -*, Phys. Rev. D **82** (2010) 054018, [arXiv:1005.4451](https://arxiv.org/abs/1005.4451) [hep-ph].

[44] T. Gleisberg et al., *Event generation with SHERPA 1.1*, JHEP **0902** (2009) 007, [arXiv:0811.4622](https://arxiv.org/abs/0811.4622) [hep-ph].

[45] T. Gleisberg and S. Höche, *Comix, a new matrix element generator*, JHEP **0812** (2008) 039, [arXiv:0808.3674](https://arxiv.org/abs/0808.3674) [hep-ph].

[46] F. Caccioli, P. Maierhofer, and S. Pozzorini, *Scattering Amplitudes with Open Loops*, Phys. Rev. Lett. **108** (2012) 111601, [arXiv:1111.5206](https://arxiv.org/abs/1111.5206) [hep-ph].

[47] S. Schumann and F. Krauss, *A Parton shower algorithm based on Catani-Seymour dipole factorisation*, JHEP **0803** (2008) 038, [arXiv:0709.1027](https://arxiv.org/abs/0709.1027) [hep-ph].

[48] S. Höche, F. Krauss, M. Schönherr, and F. Siegert, *QCD matrix elements + parton showers: The NLO case*, JHEP **1304** (2013) 027, [arXiv:1207.5030](https://arxiv.org/abs/1207.5030) [hep-ph].

[49] R. Gavin, Y. Li, F. Petriello, and S. Quackenbush, *FEWZ 2.0: A code for hadronic  $Z$  production at next-to-next-to-leading order*, Comput. Phys. Commun. **182** (2011) 2388, [arXiv:1011.3540](https://arxiv.org/abs/1011.3540) [hep-ph].

[50] D. J. Lange, *The EvtGen particle decay simulation package*, Nucl. Instrum. Meth. A **462** (2001) 152.

[51] P. Z. Skands, *Tuning Monte Carlo Generators: The Perugia Tunes*, *Phys. Rev. D* **82** (2010) 074018, [arXiv:1005.3457](https://arxiv.org/abs/1005.3457) [hep-ph].

[52] S. Gieseke, C. Rohr, and A. Siodmok, *Colour reconnections in Herwig++*, *Eur. Phys. J. C* **72** (2012) 2225, [arXiv:1206.0041](https://arxiv.org/abs/1206.0041) [hep-ph].

[53] A. Martin, W. Stirling, R. Thorne, and G. Watt, *Update of parton distributions at NNLO*, *Phys. Lett. B* **652** (2007) 292, [arXiv:0706.0459](https://arxiv.org/abs/0706.0459) [hep-ph].

[54] ATLAS Collaboration, *Summary of ATLAS Pythia 8 tunes*, ATL-PHYS-PUB-2012-003, 2012, <https://cds.cern.ch/record/1474107>.

[55] ATLAS Collaboration, *Vertex Reconstruction Performance of the ATLAS Detector at  $\sqrt{s} = 13$  TeV*, ATL-PHYS-PUB-2015-026, 2015, <https://cds.cern.ch/record/2037717>.

[56] ATLAS Collaboration, *Topological cell clustering in the ATLAS calorimeters and its performance in LHC Run 1*, [arXiv:1603.02934](https://arxiv.org/abs/1603.02934) [hep-ex], submitted to *Eur. Phys. J. C*.

[57] M. Cacciari, G. P. Salam, and G. Soyez, *The Anti- $k(t)$  jet clustering algorithm*, *JHEP* **0804** (2008) 063, [arXiv:0802.1189](https://arxiv.org/abs/0802.1189) [hep-ph].

[58] ATLAS Collaboration, *Jet energy scale measurements and their systematic uncertainties in proton-proton collisions at  $\sqrt{s} = 13$  TeV with the ATLAS detector*, [arXiv:1703.09665](https://arxiv.org/abs/1703.09665) [hep-ex].

[59] ATLAS Collaboration, *Selection of jets produced in 13 TeV proton–proton collisions with the ATLAS detector*, ATLAS-CONF-2015-029, 2015, <https://cds.cern.ch/record/2037702>.

[60] ATLAS Collaboration, *Performance of pile-up mitigation techniques for jets in pp collisions at  $\sqrt{s} = 8$  TeV using the ATLAS detector*, *Eur. Phys. J. C* **76** (2016) 581, [arXiv:1510.03823](https://arxiv.org/abs/1510.03823) [hep-ex].

[61] ATLAS Collaboration, *Jet Calibration and Systematic Uncertainties for Jets Reconstructed in the ATLAS Detector at  $\sqrt{s} = 13$  TeV*, ATL-PHYS-PUB-2015-015, 2015, <https://cds.cern.ch/record/2037613>.

[62] ATLAS Collaboration, *Performance of b-Jet Identification in the ATLAS Experiment*, *JINST* **11** (2016) P04008, [arXiv:1512.01094](https://arxiv.org/abs/1512.01094) [hep-ex].

[63] ATLAS Collaboration, *Optimisation of the ATLAS b-tagging performance for the 2016 LHC Run*, ATL-PHYS-PUB-2016-012, 2016, <https://cds.cern.ch/record/2160731>.

[64] ATLAS Collaboration, *Electron reconstruction and identification efficiency measurements with the ATLAS detector using the 2011 LHC proton–proton collision data*, *Eur. Phys. J. C* **74** (2014) 2941, [arXiv:1404.2240](https://arxiv.org/abs/1404.2240) [hep-ex].

[65] ATLAS Collaboration, *Electron and photon energy calibration with the ATLAS detector using LHC Run 1 data*, *Eur. Phys. J. C* **74** (2014) 3071, [arXiv:1407.5063](https://arxiv.org/abs/1407.5063) [hep-ex].

[66] ATLAS Collaboration, *Electron identification measurements in ATLAS using  $\sqrt{s} = 13$  TeV data with 50 ns bunch spacing*, ATL-PHYS-PUB-2015-041, 2015, <https://cds.cern.ch/record/2048202>.

[67] ATLAS Collaboration, *Muon reconstruction performance of the ATLAS detector in proton–proton collision data at  $\sqrt{s} = 13$  TeV*, *Eur. Phys. J. C* **76** (2016) 292, [arXiv:1603.05598](https://arxiv.org/abs/1603.05598) [hep-ex].

[68] ATLAS Collaboration, *Measurement of the  $t\bar{t}$  production cross-section using  $e\mu$  events with  $b$ -tagged jets in  $pp$  collisions at  $\sqrt{s} = 13$  TeV with the ATLAS detector*, *Phys. Lett. B* **761** (2016) 136, [arXiv:1606.02699 \[hep-ex\]](https://arxiv.org/abs/1606.02699).

[69] ATLAS Collaboration, *Performance of algorithms that reconstruct missing transverse momentum in  $\sqrt{s} = 8$  TeV proton–proton collisions in the ATLAS detector*, *Eur. Phys. J. C* **77** (2017) 241, [arXiv:1609.09324 \[hep-ex\]](https://arxiv.org/abs/1609.09324).

[70] ATLAS Collaboration, *Jet energy measurement with the ATLAS detector in proton–proton collisions at  $\sqrt{s} = 7$  TeV*, *Eur. Phys. J. C* **73** (2013) 2304, [arXiv:1112.6426 \[hep-ex\]](https://arxiv.org/abs/1112.6426).

[71] ATLAS Collaboration, *Measurement of the photon identification efficiencies with the ATLAS detector using LHC Run-1 data*, *Eur. Phys. J. C* **76** (2016) 666, [arXiv:1606.01813 \[hep-ex\]](https://arxiv.org/abs/1606.01813).

[72] D. R. Tovey, *On measuring the masses of pair-produced semi-invisibly decaying particles at hadron colliders*, *JHEP* **0804** (2008) 034, [arXiv:0802.2879 \[hep-ph\]](https://arxiv.org/abs/0802.2879).

[73] ATLAS Collaboration, *Search for direct third-generation squark pair production in final states with missing transverse momentum and two  $b$ -jets in  $\sqrt{s} = 8$  TeV  $pp$  collisions with the ATLAS detector*, *JHEP* **10** (2013) 189, [arXiv:1308.2631 \[hep-ex\]](https://arxiv.org/abs/1308.2631).

[74] A. J. Barr, B. Gripaios, and C. G. Lester, *Transverse masses and kinematic constraints: from the boundary to the crease*, *JHEP* **11** (2009) 096, [arXiv:0908.3779 \[hep-ph\]](https://arxiv.org/abs/0908.3779).

[75] P. Konar, K. Kong, K. T. Matchev, and M. Park, *Dark Matter Particle Spectroscopy at the LHC: Generalizing  $M(T2)$  to Asymmetric Event Topologies*, *JHEP* **04** (2010) 086, [arXiv:0911.4126 \[hep-ph\]](https://arxiv.org/abs/0911.4126).

[76] C. G. Lester and D. J. Summers, *Measuring masses of semiinvisibly decaying particles pair produced at hadron colliders*, *Phys. Lett. B* **463** (1999) 99–103, [arXiv:hep-ph/9906349 \[hep-ph\]](https://arxiv.org/abs/hep-ph/9906349).

[77] M. Baak et al., *HistFitter software framework for statistical data analysis*, *Eur. Phys. J. C* **75** (2015) 153, [arXiv:1410.1280 \[hep-ex\]](https://arxiv.org/abs/1410.1280).

[78] ATLAS Collaboration, *Search for squarks and gluinos with the ATLAS detector in final states with jets and missing transverse momentum using  $4.7\text{ fb}^{-1}$  of  $\sqrt{s} = 7$  TeV proton–proton collision data*, *Phys. Rev. D* **87** (2013) 012008, [arXiv:1208.0949 \[hep-ex\]](https://arxiv.org/abs/1208.0949).

[79] ATLAS Collaboration, ATLAS Collaboration, *Search for squarks and gluinos in events with isolated leptons, jets and missing transverse momentum at  $\sqrt{s} = 8$  TeV with the ATLAS detector*, *JHEP* **04** (2015) 116, [arXiv:1501.03555 \[hep-ex\]](https://arxiv.org/abs/1501.03555).

[80] ATLAS Collaboration, *Studies on top-quark Monte Carlo modelling with Sherpa and MG5\_aMC@NLO*, ATL-PHYS-PUB-2017-007, <https://cds.cern.ch/record/2261938>.

[81] ATLAS Collaboration, *Jet energy resolution in proton–proton collisions at  $\sqrt{s} = 7$  TeV recorded in 2010 with the ATLAS detector*, *Eur. Phys. J. C* **73** (2013) 2306, [arXiv:1210.6210 \[hep-ex\]](https://arxiv.org/abs/1210.6210).

[82] ATLAS Collaboration, *Measurement of the cross section for the production of a  $W$  boson in association with  $b$ -jets in  $pp$  collisions at  $\sqrt{s} = 7$  TeV with the ATLAS detector*, *Phys. Lett. B* **707** (2012) 418, [arXiv:1109.1470 \[hep-ex\]](https://arxiv.org/abs/1109.1470).

- [83] M. Bähr et al., *Herwig++ Physics and Manual*, *Eur. Phys. J. C* **58** (2008) 639, [arXiv:0803.0883 \[hep-ph\]](https://arxiv.org/abs/0803.0883).
- [84] T. Junk, *Confidence level computation for combining searches with small statistics*, *Nucl. Instrum. Meth. A* **434** (1999) 435, [arXiv:hep-ex/9902006 \[hep-ex\]](https://arxiv.org/abs/hep-ex/9902006).
- [85] A. L. Read, *Presentation of search results: The  $CL(s)$  technique*, *J. Phys. G* **28** (2002) 2693.
- [86] ATLAS Collaboration, *ATLAS Computing Acknowledgements 2016–2017*, ATL-GEN-PUB-2016-002, <https://cds.cern.ch/record/2202407>.